

CFD Based Modelling
of
Proton Exchange Membrane Fuel Cells

by

Børge Rygh Sivertsen

2003

Heat and Energy Processes

Report number: 03:43

A Thesis Submitted in Partial Fulfillment of the
Requirements for the Degree of

MASTER OF SCIENCE

IN

ENERGY AND ENVIRONMENTAL ENGINEERING

at Norwegian University of Science and Technology, NTNU

Conducted at:

University of Victoria,

Institute for Integrated Energy Systems.

© BØRGE RYGH SIVERTSEN, 2003

Norwegian University of Science and Technology, NTNU

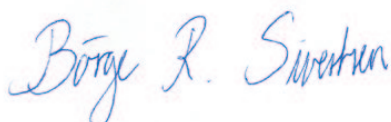
All rights reserved. This thesis may not be reproduced in whole or in part, by
photocopy or other means, without the permission of the author.

July 14, 2003, Victoria, BC, Canada

The following thesis is submitted at the Norwegian University of Science and Technology (NTNU) in partial fulfilment of the requirements for the degree in Master of Science. The research has been conducted at the Institute for Integrated Energy Systems (IESVic) at the University of Victoria, under the supervision of Dr. Djilali.

The work presented in this thesis is a direct continuation of the project conducted at the Institute for Integrated Energy Systems (IESVic) at the University of Victoria in the fall 2002. It would therefore be advantageous to possess a copy of the project when reading this thesis. However, it should be noted that there has been quite a few changes in the approach presented in the project so some topics will be covered again in this thesis.

Much time and effort has been put down into making the code run in parallel. This has been necessary in order to be able to run bigger models and to make this into an efficient design tool for fuel cells.



Børge Rygh Sivertsen

Supervisors: Prof. O. Melhus and Dr. N. Djilali

Abstract

A comprehensive non-isothermal, three-dimensional computational model of a proton exchange membrane (PEM) fuel cell has been developed. The model incorporates a straight channel fuel cell with the membrane-electrode-assembly, gas distribution flow channels and bipolar-plates. The model is implemented into a computational fluid dynamic (CFD) code, and deals with important transport phenomena taking place in the fuel cell. One of the powerful features of the implementation is parallel processing, which allows practical simulations for large computational domains. The model solves the convective and diffusive transport and allows prediction of the concentration of the species present. A distributed heat generation in both the cathode and the anode is also included in the model. The Butler-Volmer equation is used to calculate the local current density at both the cathode and at the anode. The transport of electrons in the gas diffusion electrodes is solved. In contrast to most published models, this model accounts for a distributed overpotential at the cathodic catalyst layer. This makes it possible to address the current density dependency on concentration of reactants and activation overpotential. The model shows that the local current density profile is dependent on activation overpotential and the ohmic losses in the gas diffusion electrodes. The validity of using a polarisation curve in order to verify a fuel cell model is also addressed.

Acknowledgements

I would like to thank my supervisors Ole Melhus and Ned Djilali for their supervision and support. I would especially like to thank Ned for giving me the opportunity to work on such an exiting project and to conduct my thesis at the Institute for Integrated Energy Systems, IESVic.

I want to thank everyone in the research group at IESVic and the CFD group at the University of Victoria for their help and support.

I would also like to express my appreciation for valuable guidance and discussions with Jon Pharoah, Queen's University. Torsten Berning and Mads Bang, thank you for helping me out in the start of my work.

You all contributed to making my time in Canada great.

Proposal

Background

Proton-Exchange Membrane (PEM) technology is favourably positioned for successful entry into a broad range of energy market services including transport, portable devices, stationary and residential power generation.

Increased awareness of environmental problems caused by combustion of hydrocarbon fuels, especially the emission of CO_2 , has led to an increased interest in fuel cells. Perhaps one of the most important concrete initiatives is the zero emission vehicle (ZEV) program adopted by the California Air Resources Board (ARB) in 1990. The fact that several other states also have opted to follow California's pollution rules [1], put huge pressure on the automobile industry to increase their efforts towards developing fuel cell technology.

Fuel cells are electrochemical devices that allow the chemical energy of the fuel to be converted into electrical power without direct combustion as an intermediary. Fuel cells are similar to batteries, but do not store chemical energy like a battery, and instead operate continuously as long as they are provided with reactant gases.

A Proton Exchange Membrane Fuel Cell consists of a Membrane-Electrode Assembly (MEA) sandwiched between collector plates in which are machined serpentine flow channels that distribute reactants and transport products. Several coupled fluid flow, heat and mass transport processes occur in a fuel cell. Optimal operation requires good understanding and control of the transport processes (fluid flow, heat and mass transport, phase change and electrochemistry). A fuel cell system usually includes various components (e.g. heat and water management), and better understanding of the fundamental processes in a fuel cell will lead to a shorter design cycle.

Short literature review with comments on work that is to be done

While progress in recent years has led to tremendous increase in power densities, reliability and overall performance, the underlying physics of the transport processes in a fuel cell (fluid flow, heat and mass transport, and electrochemistry) are poorly understood leaving room for optimisation. The development of physically representative models that allow reliable simulation of the processes under realistic conditions is essential to the development of better fuel cells that have optimised performance and that can be manufactured using cheaper materials and techniques.

In a fuel cell it is often very difficult perform measurements without interfering with the operation of the cell. For that reason much effort has been devoted to modelling. Fuel cell modelling has been used extensively to provide insightful information about fuel cell performance in order to understand the mechanisms within the cell. The models that were used in the early 1990s were generally one-dimensional in nature, often focusing on a small part of the cell and neglecting both heat transfer and convective transport in the flow channels. In the late 1990s the models became more complex and researchers began to apply Computational Fluid Dynamics (CFD) in their fuel cell modelling [2]. The recent use of CFD has allowed the development of increasingly realistic computational models, accounting for fluid, thermal and electrochemical transport, and also including flow channels and cooling channels.

In 1991, Bernardi and Verbrugge [3], published an isothermal one-dimensional model of an ion-exchange membrane attached to a gas-fed porous oxygen electrode. A year later they published a one-dimensional isothermal model including both anode and cathode side [4]. Their models provided valuable information about the physics of electrochemical reactions and transport phenomena.

Springer and his colleagues at the Los Alamos National Laboratory have con-

tributed significantly through several publications to the understanding of the mechanisms in a PEM fuel cell [5]. An early study, Springer et al. 1991 [6], developed an isothermal one-dimensional model, the first to account for a partially dehumidified membrane. This was done by using experimentally determined parameters. Still, this model is widely used when partial humidification of the membrane is taken into account [2].

As a first stage a simplified membrane model will be used in this project. Depending on the progress of the work, a model based on the work by Springer et al. [6] or a model similar to the one used by Berning [2] will be implemented.

Fuller and Newman [7] were the first to publish a model that presents a quasi two-dimensional model of a membrane-electrode assembly. Their model accounted for thermal effects and was based on concentrated solution theory. The model solved transport in the cell one-dimensionally at different points and integrated the solution down the channel.

A two dimensional, steady state, heat and mass transfer model with flow channels was presented in 1993 by Nguyen and White [8]. They studied the effects of various forms of gas humidification on water management and cell performance. The model used, a simplified membrane-electrode assembly. In 1998, Yi and Nguyen published a refined version of the previous model [9]. The model included convective water transport across the membrane driven by pressure gradients. In addition, temperature distribution in the solid phase along the flow channel, and heat removal by natural convection and coflow or counterflow heat exchangers were also accounted for.

The first model that used computational fluid dynamics was developed by Gurau et al. [10] in 1998. This model was a two-dimensional, steady state model of a whole fuel cell with flow channels. Gas and liquid phases were considered in separate computational domains meaning that the interaction between the two phases was unaccounted for.

In 2000 the first fully three-dimensional model was presented by Dutta and his colleagues [11]. The isothermal, single-phase, mass transfer model was implemented in the commercial code Fluent. A year later the same group published a three-dimensional, steady state, single-phase, multi-species, isothermal mass transfer model of a whole cell with a serpentine flow channel. Except for the isothermal mass transfer and the uniform grid, this model is similar to the one that will be developed in this project. The proposed work will also involve implementing a non-constant overpotential at the cathode. Because of the complicated transport process at the cathode side of the fuel cell, the overpotential is expected to be non-uniform. This will effect the operation of the cell. At the anode side the transport process is less complex since there are fewer species present. This leads to a much more uniform overpotential. For that reason a constant overpotential will be assumed.

A non-isothermal three-dimensional computational model accounting for two-phase flow and phase change of water inside the gas diffusion layer was developed by Berning in 2002 [12] [2].

Depending on the time spent on developing a one-phase model, the proposed work might be expanded to include implementation of a two-phase model. The implementation of a good membrane model is highly related to the water management in the cell, which can only fully be understood by taking account of the phase change in the cell.

Another interesting topic that might be investigated further if time permits, is a sensitivity analysis of the fuel cell model. The parameters that govern transport in all applications are known only to a certain level of accuracy. Assessing the flow, thermal or electrochemical response to these uncertainties is very important in order to make a good design [13][14].

There also some issues related to the fuel used in the cell that should be more thoroughly studied. If the hydrogen used comes from a fuel reforming system, it will

normally contain some carbon monoxide. Even small amounts of carbon monoxide have a great affect on the anode. Carbon monoxide occupies platinum catalyst sites, preventing hydrogen fuel from reacting [15]. The effect of carbon monoxide poisoning would also be very interesting to include in the model if the time permits.

Objective of Thesis

This thesis will continue the work started in the project [16] conducted at the Institute for Integrated Energy Systems (IESVic) at the University of Victoria in the fall 2002. In the project [16] the background for building a Polymer Electrolyte Membrane (PEM) fuel cell model was investigated. A basic test model of fuel cell was implemented in FLUENT 6.0. The proposed project will complete the work to develop a single-phase three-dimensional model of a complete fuel cell with serpentine flow channels.

As a first stage, only a single-phase model will be investigated. A single-phase model will only be adequate for small current densities. At higher current densities a two-phase model will be necessary [17]. The transport processes becomes much more complex due to the coupled flow of liquid water and gas in the porous media. However, a single-phase model will give a good indication of the water fluxes and the saturation pressure will indicate where liquid water is formed.

The goal of the model is to provide information which is not measurable, and thereby increase the understanding of the processes taking place in the cell. A computation model would be an important design tool for rapid parametric studies, analysis and optimisation. The results will be compared with results either from a fuel cell in the laboratory at the University of Victoria or results provided by BallardTM. If the time permits, a parametric study of the fuel cell will also be preformed.

It is expected that in addition to the thesis submitted at NTNU, the work will

result in a paper to be presented at an appropriate conference and at least one paper to be submitted to an appropriate journal.

Supervisors: Prof. O. Melhus and Dr. N. Djilali

Table of Contents

Letter of Transmittal	ii
Abstract	iii
Proposal	v
List of Tables	xiii
List of Figures	xiv
List of Symbols	xvi
1 Introduction	1
1.1 Scope of the Thesis	2
1.2 Thesis Layout	3
1.3 Basic Principles of a Proton Exchange Membrane Fuel Cell [16] . . .	4
2 Three-Dimensional Fuel Cell Model	6
2.1 This Model	6
2.2 Assumptions	7
2.3 Modelling Equations	9
2.3.1 Flow channel	9
2.3.2 Gas diffusion layers	12
2.3.3 Catalyst layer	15
2.3.4 Membrane	23
2.4 Boundary Conditions	28
2.4.1 Inlet conditions	28
2.4.2 Outlet conditions	32
2.4.3 Boundary conditions at internal interfaces	33
2.4.4 Land areas	34
2.4.5 Walls	34

2.5	Computational Procedure	36
2.5.1	Parallel solver	38
2.6	Summary	40
3	Straight Channel Test Case	41
3.1	Modelling Parameters	42
3.2	Grid Study	47
4	Results and Discussion	51
4.1	Polarisation Curve	51
4.2	Velocity Contours	58
4.3	Concentrations of Reactants	60
4.4	Temperature Distribution	63
4.5	Current Density Distribution	66
4.5.1	Discussion	71
4.6	Losses	73
4.6.1	Ohmic losses in the electrodes	73
4.6.2	Ohmic losses in the membrane	75
4.6.3	Relative share of different losses	76
5	Conclusions and Future Work	78
5.1	Conclusions	78
5.2	Future Work	80
	References	82
A	Half-cell Voltage	88
B	Heat and Entropy for Half-cell Reactions	94
C	Fluid Properties	99

List of Tables

2.1	Discretisation schemes for the scalars used in this model	37
3.1	Physical dimensions for the straight channel case	42
3.2	Operation parameters for the straight channel case	44
3.3	Mass fraction at the inlets, fully humidified flow	44
3.4	Electrode properties for the straight channel case	45
3.5	Membrane properties for the straight channel case	46
3.6	Computational grid parameters	48
4.1	Polarisation data provided by the model, $\beta = 1$	52
4.2	Polarisation data provided by the model, $\beta = 0.5$	52
C.1	Fluid properties used in this model [18], $T = 353.15K$	99

List of Figures

1.1	Basic principle of a fuel cell [15]	4
2.1	Schematic drawing of the cathodic side of the FC model	12
2.2	Velocity profile for a square channel, $\frac{a}{b} = 1$	31
2.3	Solver algorithm	36
2.4	FLUENT parallel architecture [19]	40
3.1	Cross-section of the computational grid	43
3.2	Relative difference in the local current density between grids C and A (Reference grid A)	50
3.3	Relative difference in the local current density between grids B and A (Reference grid A)	50
4.1	Polarisation curve	53
4.2	Cathodic current density, $\beta = 1.0$	56
4.3	Cathodic current density, $\beta = 0.5$	56
4.4	Relative difference between the current density profiles with $\beta = 1.0$ and $\beta = 0.5$ (Reference $\beta = 0.5$)	57
4.5	Graphical representation of the Butler-Volmer equation, with different asymmetry parameters	57
4.6	Velocity profiles $0.989A/cm^2$, $\beta = 0.5$ (outlet in foreground)	59
4.7	Mass fractions of oxygen, $0.2691A/cm^2$, $\beta = 0.5$ (outlet in foreground)	61
4.8	Mass fractions of hydrogen, $0.2691A/cm^2$, $\beta = 0.5$ (outlet in foreground)	62
4.9	Temperature profiles in a cross-section of the fuel cell with two different boundary conditions (top channel corresponds to anode)	64
4.10	Relative difference in the local current density between the simula- tions using two different temperature boundaries (Reference constant temperature boundaries)	65
4.11	Profiles for current density, activation overpotential and oxygen mass fraction at the cathode catalyst layer at $V_{ref} = 15.444V$, $\beta = 0.5$	66

4.12	Profiles for current density, activation overpotential and oxygen mass fraction at the cathode catalyst layer at $V_{ref} = 15.405V$, $\beta = 0.5$. . .	67
4.13	Plots of the relative current densities (i_{local}/i_{avg}) for different conductivities	70
4.14	Magnified image of a gas diffusion electrode (Reproduced by premission from B. Peppley [20])	72
4.15	Potential profile through the cathodic diffusion electrode shown at a cross-section at the centre of the channel, $V_{ref} = 15.405V$, $\beta = 0.5$. .	74
4.16	Potential profile through the anodic diffusion electrode shown at a cross-section at the centre of the channel, $V_{ref} = 15.405V$, $\beta = 0.5$. .	74
4.17	Potential profile through the membrane shown at a cross-section at the centre of the channel, $V_{ref} = 15.405V$, $\beta = 0.5$	75
4.18	Share of overpotential contributions at $V_{ref} = 15.444V$, $\beta = 1.0$, $i_{avg} = 0.299A/cm^2$	76
4.19	Share of overpotential contributions at $V_{ref} = 15.444V$, $\beta = 0.5$, $i_{avg} = 0.299A/cm^2$	76
4.20	Share of overpotential contributions at $V_{ref} = 15.405V$, $\beta = 0.5$, $i_{avg} = 0.989A/cm^2$	77

List of Symbols

Symbol	Description	Units
a	Chemical activity	-
A	Area	m^2
C_{ij}	Inertial resistance coefficients	-
c	Concentration	mol/m^3
D_{ij}	Binary diffusion coefficient	m^2/s
E	Energy	J
E_r	Reversible cell potential	V
E°	Standard open circuit voltage	V
F	Faraday's constant	C/mol
G	Gibb's free energy	J
g	Gravity	m/s^2
H	Enthalpy	J
h	Specific enthalpy	J/kg
I	Current	A
i	Local current density	A/m^3
i_0	Local exchange current density	A/m^3
\mathbf{j}	Diffusive mass flux vector	$kg/(s \cdot m^2)$
j	Current density of protons	A
k	Thermal conductivity	$W/m \cdot K$
$k_0^{+/-}$	Electrochemical rate constants	m/s
L	Onsager coefficient	-
l_{mem}	Permeability in the membrane	$mol^2 \cdot s / (m^3 \cdot kg)$
M	Molecular weight	kg/mol
\dot{m}	Mass flow rate	kg/s
N	Flux	mol/s
n	Number of electrons per mol of reactant	-
p	Pressure	Pa
\dot{Q}	Heat flux	W

Symbol	Description	Units
R	Universal gas constant	$J/(mol \cdot K)$
r	Specific electric resistance	Ω/m^3
S	Volumetric source term	-
S	Entropy	J/K
T	Temperature	K
t_w	Transport number of water	-
u	Velocity x-component	m/s
u_m	Mean axial velocity	m/s
V	Volume	m^3
V	Voltage	V
V_{ki}	Atomic diffusion volume	m^3
\mathbf{v}	Velocity vector	m/s
v	Velocity y-component	m/s
w	Velocity z-component	m/s
x	Mol fraction	-
y	Mass fraction	-
α	Permeability	m^2
β	Asymmetry parameter	-
γ	Porosity	-
η	Overpotential	V
κ	Specific proton conductivity of the membrane	S/m
λ	Water content in the membrane	-
λ	Stoichiometric flow rate	-
μ	Dynamic viscosity	$kg/(m \cdot s)$
μ	Chemical potential	J/mol
μ_p	Tortuosity factor	-
ξ	Number of water molecules per proton in the electro-osmotic flow	
ρ	Density	kg/m^3
σ	Electronic conductivity	S/m
τ	Viscous stress	N/m^2
ϕ	Potential	V

Chapter 1

Introduction

Fuel Cells are electrochemical devices that allow the chemical energy of the fuel to be converted into electrical power without direct combustion as a intermediary. Fuel cells are similar to batteries, but do not store chemical energy like a battery does, but rather operate continuously as long as they are provided with reactant gases.

Contrary to popular opinion, fuel cell technology is not a new invention. The first demonstration of the fuel cell operating principle was performed by William Grove in 1839 [15]. In contrast, N. A. Otto built a successful four-stroke engine in 1876, using the cycle proposed by Beau de Rochas in 1862 [21], a development which led to today's internal combustion engine.

However, even though fuel cells are not a new invention, the processes taking place inside the fuel cell are not fully understood.

1.1 Scope of the Thesis

The scope of this thesis has been slightly altered since the proposal was written. In the process of developing the fuel cell model, novel results were obtained and deemed sufficiently interesting to warrant further investigation. That research was conducted at the expense of developing a complete fuel cell with serpentine flow channels. Instead, the effect of variable overpotential has been thoroughly studied. Much effort has also been devoted to designing the code for parallel processing, which makes the model an effective design tool that can provide good results faster.

The results obtained from the model have been compared to experimental data provided by H. Lui et al. [22], and not with results from a fuel cell in the laboratory at the University of Victoria or results provided by BallardTM as indicated in the proposal.

Due to time limitations neither implementation of a two-phase model, sensitivity analysis nor carbon monoxide poisoning has been implemented, but the following have been achieved:

- A comprehensive PEM fuel cell model was implemented from scratch in Fluent
- The model includes: convective and diffusive transport of species, heat transfer, distributed heat generation, calculation of half cell potentials, electrochemical reactions determined by Butler-Volmer equation, transport of electrons through the gas diffusion electrodes, distributed overpotential at the cathode, potential profile and water transport through the membrane
- The model was parallelised
- The capabilities of the model were demonstrated by comparison with available experimental data

- The model was applied to perform some parametric studies and to investigate fundamental aspects of the transport processes in the gas diffusion electrodes.

1.2 Thesis Layout

This thesis is comprised of 5 chapters. Chapter 1 introduces the problem being studied, the associated motivation and the scope of the thesis. This chapter is condensed down to a minimum since the content was thoroughly presented in the project [16], which was conducted at University of Victoria, Institute for Integrated Energy Systems, in partial fulfilment of the requirements for the degree in Master of Science.

Chapter 2 presents the theory and the equations used in the model. Also, some of the contents in this chapter were presented in the project [16], but there has been several changes so a complete presentation of the model was required. The first part of the chapter describes the physics of the one-phase, three-dimensional, non-isothermal model with variable overpotential at the cathodic catalyst layer and distributed heat generation. Validation of the fluid flow is not included since this was discussed in the project [16]. Finally, the computation procedure is briefly presented.

Chapter 3 and 4 is dedicated to the study of a straight channel fuel cell test case. In chapter 3 the modelling parameters and a grid study are presented. Chapter 4 presents a verification of the fuel cell model developed. There are no straight forward ways of verifying a fuel cell model. Usually a polarisation curve is used in order to compare results from a model with experimental results. This is not a good way of verifying the model, so further analysis has been preformed. However, the results provided by this model have been compared with experimentally determined polarisation data provided by H. Liu and his group at University of Miami [22].

Finally, chapter 5 summarises the conclusions and observations from the numerical

simulations.

1.3 Basic Principles of a Proton Exchange Membrane Fuel Cell [16]

In a fuel cell, hydrogen and oxygen are reacted, and an electric current is being produced. In order to understand how the reaction between oxygen and hydrogen can produce electricity, the separate reactions on each electrode need to be considered. The fuel cell consists of two electrodes, a negatively charged anode and a positive cathode, on each side of a proton conducting membrane. The membrane serves both as an electrolyte and as a separator between reactants on the two sides. Air or pure oxygen is fed into the cathode channel, and hydrogen is fed into the anode channel. Hydrogen diffuses through the diffusion layer on the anode side towards the catalyst [16].

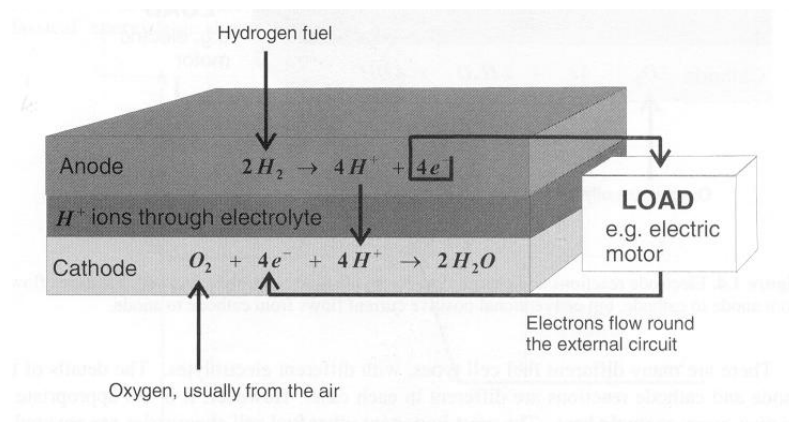
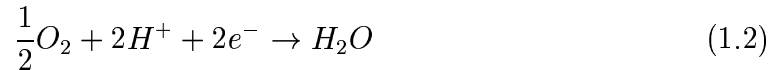


Figure 1.1: Basic principle of a fuel cell [15]

At the catalyst the hydrogen reacts according to:



Each hydrogen molecule splits up into two protons (or H^+ -ions) and two electrons. This reaction is slightly endothermic, but the heat production due to ohmic losses and reaction resistance might make the anode half cell exothermic (see equation (2.32)). The protons migrate through the membrane, and the freed electrons travel through the conductive diffusion layer and an external circuit, in the form of direct-current electricity. At the cathode, the oxygen diffuses through the diffusion layer, and reacts at the catalyst layer with the electrons and the protons from the electrolyte to form water:



This reaction is highly exothermic, so there is a net production of heat in the fuel cell [23]. If the two half cell reactions are combined, it can be seen that the overall reaction for a PEM fuel cell is given by:



A more detailed description of the different components of the fuel cell can be found in the project [16].

Chapter 2

Three-Dimensional Fuel Cell Model

The background for building a Proton Exchange Membrane (PEM) fuel cell model was investigated in the project [16] as described earlier. This thesis is based on that study, so the fundamental background will not be discussed in depth here. However, there has been some changes in the approach, so a short presentation of the equations used will be presented in this chapter.

2.1 This Model

In this thesis a one-phase, three-dimensional, non-isothermal model is presented. This model uses the commercial CFD package Fluent 6.1, with custom-developed user-subroutines that take account of the physics which Fluent 6.1 is not capable of. The Butler-Volmer equation is used to calculate the local current density at both the cathode and anode. A variable exchange current density dependent on the local

temperature and concentration of reactants is applied. In contrast to most published models, this model accounts for a distributed overpotential at the cathodic catalyst layer. This model also takes into account the convection and diffusion of different species in the channels as well as in the porous gas diffusion layer, heat transfer in the solids as well as the gases, electrochemical reactions and the transport of liquid water through the membrane. The governing input parameter in this model is the cathodic half-cell potential instead of the average current, which is used in many other models.

2.2 Assumptions

As any other model, this one is based on several assumptions and simplifications. The main assumptions used in this model are briefly presented in this section:

- The fuel cell operates under steady-state conditions
- The flow in the channels is laminar
- Dilute solution theory is used to determine the species diffusion
- All gases are assumed to be non-compressible ideal gases
- The model presented is a one-phase model
- All water produced in the electrochemical reactions is assumed to be in the gas phase
- The membrane is assumed to be fully humidified so the electronic conductivity is taken to be constant

- The membrane is considered impermeable for the the gases, so cross-over of reactant gases can be neglected [4]
- Ohmic heating in the bipolar plates and in the gas diffusion electrodes is neglected due to high conductivity.
- Ohmic heating is neglected in the membrane at this stage. Heat transfer in the membrane is assumed to take place due to conduction only
- Electro-neutrality prevails inside the membrane. The proton concentration in the membrane is assumed to be constant and equal to the concentration of fixed sulfonic acid groups
- The overpotential at the anode is assumed to be constant
- First order kinetics are used to calculate the exchange current density
- The gas diffusion layer is assumed to be homogeneous and isotropic

2.3 Modelling Equations

2.3.1 Flow channel

CFD codes are structured around numerical algorithms that use physical conservation laws to solve the fluid problems. In this section the equations related to the flow channels in the fuel cell are presented:

Continuity

The three-dimensional steady state continuity equation is given by [24]

$$\frac{\partial(\rho u)}{\partial x} + \frac{\partial(\rho v)}{\partial y} + \frac{\partial(\rho w)}{\partial z} = 0 \quad (2.1)$$

where ρ is the density and u , v and w are the velocities in the x , y and z direction, respectively. The density of each specie is calculated using the following relation:

$$\rho_i = \frac{p_{op} \cdot M_i}{RT} \quad (2.2)$$

in which p_{op} is a constant and is equal to the anode or the cathode side pressure. M_i is the molecular weight, T is the temperature and R is the universal gas constant.

The density of the mixture is calculated using [19]:

$$\rho = \frac{1}{\sum_i \frac{y_i}{\rho_i}} \quad (2.3)$$

where y_i is the mass fraction of specie i .

Navier-Stokes

The flow field can be calculated using the steady state Navier-Stokes equations with internal source terms [25][24]:

$$\begin{aligned}
\rho u \frac{\partial u}{\partial x} + \rho v \frac{\partial u}{\partial y} + \rho w \frac{\partial u}{\partial z} &= -\frac{\partial p}{\partial x} + \rho g_x + \mu \left(\frac{\partial^2 u}{\partial x^2} + \frac{\partial^2 u}{\partial y^2} + \frac{\partial^2 u}{\partial z^2} \right) + S_x \\
\rho u \frac{\partial v}{\partial x} + \rho v \frac{\partial v}{\partial y} + \rho w \frac{\partial v}{\partial z} &= -\frac{\partial p}{\partial y} + \rho g_y + \mu \left(\frac{\partial^2 v}{\partial x^2} + \frac{\partial^2 v}{\partial y^2} + \frac{\partial^2 v}{\partial z^2} \right) + S_y \\
\rho u \frac{\partial w}{\partial x} + \rho v \frac{\partial w}{\partial y} + \rho w \frac{\partial w}{\partial z} &= -\frac{\partial p}{\partial z} + \rho g_z + \mu \left(\frac{\partial^2 w}{\partial x^2} + \frac{\partial^2 w}{\partial y^2} + \frac{\partial^2 w}{\partial z^2} \right) + S_z
\end{aligned} \tag{2.4}$$

where p is the pressure as a function of x , y and z direction, g is the gravity, μ is the dynamic viscosity and S is the source of momentum per unit volume per unit time.

Transport equations

The steady state transport equation takes the following general form [19]:

$$\nabla \cdot (\rho \mathbf{v} y_i) = -\nabla \cdot \mathbf{j}_i + S_i \tag{2.5}$$

where y_i is the mass fraction of specie i , \mathbf{j}_i is the diffusive mass flux vector and S_i is a source term.

Multicomponent effects are usually considered to be small in dilute solutions and in solutions where the species are of similar size and nature [26] [27]. In order to account for the tortuosity in the porous media in the electrodes, the dilute diffusion model had to be used. In Fluent there is no straight forward way of taking into account the tortuosity when the Maxwell-Stefan equations are applied.

The diffusive mass flux vector \mathbf{j}_i can be written as [19] [16]:

$$\mathbf{j}_i = - \sum_{j=1}^{N-1} \rho D_{ij} \nabla y_j \quad (2.6)$$

where D_{ij} is the binary-diffusion coefficient. See reference [16] for a more detailed description of diffusion.

The binary diffusion coefficients are dependent on temperature and pressure. They can be calculated according to the empirical relation [26]:

$$D_{ij} = \frac{T^{1.75} (1/M_i + 1/M_j)^{1/2}}{p \left((\sum_k V_{ki})^{1/3} + (\sum_k V_{kj})^{1/3} \right)^2} \cdot 10^{-3} \quad (2.7)$$

where D_{ij} is the binary diffusion coefficient, T is the temperature in Kelvin, p is the pressure in atmospheres, M_i is the molecular weight of species i and V_{ki} is the atomic diffusion volume. The values for $\sum V_{ki}$ is given by Cussler [26].

Energy equation

The energy equation is derived from the first law of thermodynamics, which states that the rate of change in energy of a fluid particle equals the sum of the rate of heat transferred to the fluid particle and the rate of work done on the particle. The steady state energy equation can be expressed as [19]:

$$\nabla \cdot (\mathbf{v}(\rho E + p)) = \nabla \cdot \left(k_{eff} \nabla T - \sum_j h_j \mathbf{j}_j + (\tau_{eff} \cdot \mathbf{v}) \right) + S_h \quad (2.8)$$

where k_{eff} is the effective conductivity, and \mathbf{j}_j is the diffusion flux of species j and h is the enthalpy, τ_{eff} is the effective stress tensor matrix and S_h is the source term per unit volume per unit time. However, the dissipation energy will be very low in the fuel

cell due to low velocity laminar flow and can be omitted from the energy equation. The first three terms on the right-hand side of equation (2.8) represent the energy transfer due to conduction, species diffusion, and viscous dissipation, respectively.

2.3.2 Gas diffusion layers

The gas diffusion layers (also called the gas diffusion electrodes or only electrodes) consists of carbon cloth or carbon fibre paper and can be considered as a porous media. The gas diffusion layer serves as a current collector that connects the reaction zone with the bipolar plates. At the same time it distributes the reactant gases to the catalyst layer. The equations that govern the gas transport phenomena in the diffusion layer are similar to the equations used in the channels.

Figure 2.1 shows a schematic drawing of the cathode side of the fuel cell model [16]. The figure shows a cross-section of the geometry, with arrows indicating the transport of reactants, electrons and products.

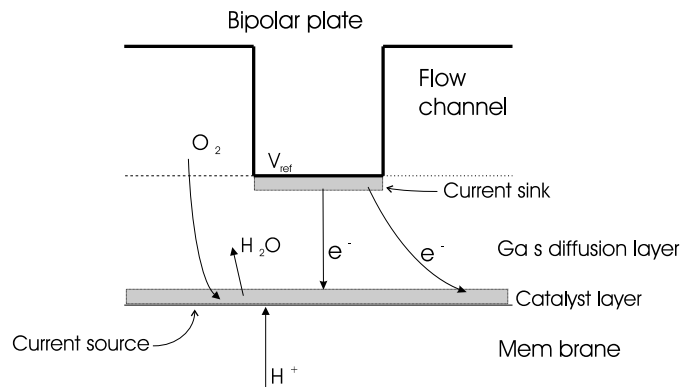


Figure 2.1: Schematic drawing of the cathodic side of the FC model

Continuity in porous media

The mass conservation equation for a porous media can be expressed as:

$$\nabla \cdot (\rho \gamma \mathbf{v}) = S_m \quad (2.9)$$

in which γ is the porosity and S_m is a mass source.

Momentum equation in porous media

Fluent 6.0 applies a superficial velocity inside the porous medium, based on the volumetric flow rate. This superficial velocity was also used to ensure continuity of the velocity vectors across the porous medium interface. For more accurate simulations of porous media flows, it becomes necessary to solve for the physical velocity throughout the flow-field, rather than the superficial velocity. Fluent 6.1 gives the possibility to solve the transport equation in the porous media using the physical velocity. However, the inlet mass flow is calculated from the superficial velocity and therefore the pressure drop across the porous media will be the same whether the physical or superficial velocity formulation is used [19].

The porous media model in Fluent is essentially nothing more than an extra momentum sink term added to the standard fluid flow equation (see equations (2.5) [19]). The source term consist of two loss terms, viscous and inertial:

$$S_i = - \left(\sum_{j=1}^3 D_{ij} \mu v_j + \sum_{j=1}^3 C_{ij} \frac{1}{2} \rho v_j v_j \right) \quad (2.10)$$

where S_i is the source term for the momentum equation in the x, y or z direction, C is the inertial resistance factor matrix and D is a matrix containing the inverse of the permeability, α . Note that the inertial loss is only significant for high flow velocities,

and is not used in this model. The momentum sink gives a pressure gradient in the porous region. The steady state momentum equation in the porous media using the physical velocity formulation can then be written as [19] [24]:

$$\nabla \cdot (\gamma \rho \mathbf{v} \mathbf{v}) = -\gamma \nabla \mathbf{p} + \nabla \gamma \tau - \frac{\mu}{\alpha} \mathbf{v} + S_{mom} \quad (2.11)$$

where τ is viscous stress tensor matrix and S_{mom} is a momentum source.

Transport equation in porous media

The steady state species transport equation in porous media becomes:

$$\nabla \cdot (\rho \gamma \mathbf{v} y_i) - \nabla \cdot (\rho \gamma D_{ii} \nabla y_i) = \nabla \cdot (\rho \gamma D_{ij} \nabla y_i) + S_i \quad (2.12)$$

The diffusion coefficient will be affected when the diffusion takes place in a porous media. In order to take account of the additional drag by the irregular shape and the actual length of the pores in comparison with a bundle of straight parallel capillaries with constant diameter, a effective diffusion coefficient D^{eff} is introduced [28] [26]:

$$D_{ij}^{eff} = \gamma \frac{D_{ij}}{\mu_p} \quad (2.13)$$

where D_{ij} is the diffusion coefficient, γ is the gas-phase porosity and μ_p is the tortuosity factor. The tortuosity factor can be divided into a factor that accounts for the actual length of the channel μ_L , and a shape factor μ_F , ($\mu_p = \mu_L \mu_F^2$) [28].

Energy equation in porous media

In the porous media equation (2.8) is used to calculate the energy transport. However, E is used as the total fluid energy.

In Fluent the effective thermal conductivity, k_{eff} , is calculated as the volume average of the fluid conductivity and the solid conductivity (assuming thermodynamic equilibrium) [19]:

$$k_{eff} = \gamma k_f + (1 - \gamma) k_s \quad (2.14)$$

where k_f is the thermal conductivity in the fluid phase and k_s is the solid medium thermal conductivity.

Potential

The potential distribution in the gas diffusion layer can be calculated by applying the generic transport equation without the convective terms.

$$-\nabla \cdot (\sigma \nabla \phi) = S_\phi \quad (2.15)$$

where σ is the electronic conductivity. The source term, S_ϕ , is equal to the local current production which is given in equation (2.19). ϕ is the potential at each location.

2.3.3 Catalyst layer

In order to enhance the electrochemical reaction rates, a catalyst is needed. Platinum particles are usually used as a catalyst, both at the anode and at the cathode.

Mass sources and sinks

The electrochemical half-cell reactions in the fuel cell are given in equation (1.1) and (1.2). Based on these equations the local sinks and sources of the species can

be determined. The local volumetric sink and source terms for the electrochemical reactions can be given as a function of the local current density, i [11]. When the current density is given per unit volume, the hydrogen sink term becomes:

$$S_{H_2} = -\frac{M_{H_2}}{2F}i \quad [kg/s \cdot m^3] \quad (2.16)$$

where M_{H_2} is the molar mass of hydrogen and F is Faraday's constant.

The oxygen sink term becomes:

$$S_{O_2} = -\frac{M_{O_2}}{4F}i \quad [kg/s \cdot m^3] \quad (2.17)$$

where M_{O_2} is the molar mass of oxygen.

The water source term becomes:

$$S_{H_2O} = \frac{M_{H_2O}}{2F}i \quad [kg/s \cdot m^3] \quad (2.18)$$

where M_{H_2O} is the molar mass of water. In this one-phase model, it is assumed that all the water produced is in vapour form. The source terms presented need to be added to both the continuity equation and the transport equation.

Current calculations

Both at the cathode and the anode, the current density is calculated using the Butler-Volmer equation [29]:

$$i = i^+ + i^- = i_0 \left[\exp\left(\frac{\beta n F \eta}{RT}\right) - \exp\left(-\frac{(1 - \beta) n F \eta}{RT}\right) \right] \quad (2.19)$$

where i_0 is the exchange current density, n is the number of electrons per mol of reactant, η is the local overpotential and R is the universal gas constant. β is the asymmetry parameter, which is experimentally found to usually be between 0.4 and 0.6 [29].

There is a constant flow of electrons to and from the electrolyte at the electrodes. If it is assumed that the reaction takes place in one global step, the general process can be written as:



in which “Ox” and “Red” indicates respectively oxidised and reduced species.

At equilibrium, the forward and the reverse reaction on an electrode must take place at the same rate. In general these rates are not zero, because the rest potential, E_r corresponds to a dynamic equilibrium [29]. At rest potential, when the net current is zero, the two partial currents (resulting from the forward and reverse processes) must be equal in absolute value. This magnitude is often called the exchange current density, i_0 [29]. The exchange current density can be considered as the current density when the overpotential begins to move from zero. If the exchange current density is high, the surface of the electrode is more “active”. The exchange current density can therefor be interpreted as a measure of the activity of the electrode. The performance of a fuel cell is dependent on the exchange current density [15]. The exchange current density is given by [29]:

$$\begin{aligned} i_0 &= -i^-(E_r) = -nFc_{Ox}k_0^- \cdot \exp\left(-\frac{(1-\beta)nFE_r}{RT}\right) \\ &= i^+(E_r) = nFc_{Red}k_0^+ \cdot \exp\left(\frac{\beta nFE_r}{RT}\right) \end{aligned} \quad (2.21)$$

where k_0^- and k_0^+ are the electrochemical rate constants (m/s) [29], and c is the concentration (mol/m^3). The superscript “-” indicates transfer of electrons to the

solution species, and “+” indicates electron transfer in the opposite direction [29]. (In equation (2.19) the actual electrode potential, E , is used in the exponent, but since $E = E_r - \eta$ the exchange current density can be extracted and placed outside the brackets).

The exchange current density is commonly calculated from the following relations given by Bernardi et al. [4]:

For the cathode:

$$i_0^+ = i_0^{ref+} \left(\frac{c_{O_2}}{c_{O_2}^{ref}} \right)^{\gamma_{O_2}} \left(\frac{c_{H^+}}{c_{H^+}^{ref}} \right)^{\gamma_{H^+}^+} \quad (2.22)$$

For the anode:

$$i_0^- = i_0^{ref-} \left(\frac{c_{H_2}}{c_{H_2}^{ref}} \right)^{\gamma_{H_2}} \left(\frac{c_{H^+}}{c_{H^+}^{ref}} \right)^{\gamma_{H^+}^-} \quad (2.23)$$

where c_i is the concentration of specie i , the superscript *ref* indicates a reference state, and γ is an empirically determined concentration parameter. For the cathode it is found that; $\gamma_{O_2} = 1/2$ and $\gamma_{H^+} = 1/2$ [4]. For the anode it is found that; $\gamma_{H_2} = 1/4$ and $\gamma_{H^+} = 2$ [4].

These equations are based on the assumption of first order kinetics. This is a simplification, both the anodic and the cathodic reactions are known to take place in several steps and to have higher order kinetics. At this stage the relations presented above will be used, but a further study of the electrochemical kinetics should be performed.

In this model the concentration of protons at the catalyst surface of the anode is assumed to be constant. The equation for the exchange current density can then be simplified:

$$i_0^- = k_a \cdot (c_{H_2})^{\gamma_{H_2}} \quad (2.24)$$

where k_a is an experimentally determined constant that is dependent on the geometry

of the catalyst layer.

At the cathode side, the proton concentration at the catalyst surface is assumed to be constant (see section 2.3.4). Equation (2.22) is used in the following form:

$$i_0^+ = k_c \cdot (c_{O_2})^{\gamma_{O_2}} (c_{H^+})^{\gamma_{H^+}^+} \quad (2.25)$$

where k_c is an experimentally determined constant that is dependent on the geometry of the catalyst layer.

The mass transport losses will be incorporated in the exchange current density, because of the concentration term, and it is not needed to take additional account for these losses. When the overpotential due to mass transport losses are high, the concentration of reactants in the catalyst layer are low, and this results in a low local current density.

The exchange current density is dependent on temperature and should be corrected when a temperature other than the reference temperature is used. Parthasarathy et al. (quoted by fuller et al. [7]) has provided a relationship for the temperature dependence of the electrode kinetics of oxygen reduction:

$$i_0 = i_0(T_{ref}) \exp \left[\frac{\Delta E}{R} \left(\frac{1}{T_{ref}} - \frac{1}{T} \right) \right] \quad (2.26)$$

in which ΔE is the activation energy ($\Delta E = 73.2 kJ/mol$).

The activation overpotential stems from losses that are caused by the slowness of the reactions taking place on the surface of the electrode. Activation losses are the most important irreversibility in low and medium temperature fuel cells [15]. In the case where the electrode reaction is not fast enough to keep the system in equilibrium at the surface, the activation overpotential needs to be taken into account. In a PEM

fuel cell, the exchange current density is much larger at the anode side than at the cathode side [15].

The activation overpotential at the cathode is calculated by the following expression:

$$\eta_{act} = E_r - ir - V_{ref} \quad (2.27)$$

The overpotential must be equal to the reversible cell potential, E_r , minus the desired cathode voltage, V_{ref} . The overpotential consists of two parts: the ohmic losses and the activation overpotential. When the transport equation is applied for the electrons, the ohmic losses can be found and the remaining part will be the activation overpotential.

The reversible cell potential, E_r , can be calculated using the Nernst equation [15]. Applying Nernst equation to the cathodic half cell reaction gives (see Appendix A):

$$E_r = E^\circ - \frac{RT}{nF} \ln \left(\frac{a_{H_2O}}{a_{O_2}^{0.5} \cdot a_{H^+}^2 \cdot a_{e^-}^2} \right) \quad (2.28)$$

where E° is the open circuit voltage at standard pressure and a is the activity. It is assumed that the electrons are in their standard state and therefore that the activity is equal to 1.

The activity of the protons in the membrane is difficult to specify. The concentration of protons is assumed to be constant in the membrane (see section 2.3.4). This assumption will also suggest that the activity at the two half cell reaction should be equal. Which means that the value of the proton activity will only be important to the local heat production in the half cell reactions (see section 2.3.3), and will not effect the cell potential because it will be cancelled out.

Bernardi and Verbrugge [4] refer to experimental measurements where the fixed-

charge-site concentration in the membrane is found to be 1.2 mol/dm^3 , which is almost equal to a 1 molar solution. In “CRC Handbook of Chemistry and Physics” [30] the activity of protons in a 1 molar sulfuric acid, H_2SO_4 , solution at $25^\circ C$ is equal to 0.1316. Compared to other 1 molar solutions this is a very low number and is considered to be a worst case scenario. In this model the activity of protons is assumed to be constant and independent of the temperature.

The activity of water vapour is calculated as:

$$a_{H_2O} = \frac{p_{H_2O}}{p_{w,sat}} \quad (2.29)$$

where p_{H_2O} is the partial pressure of water vapour and $p_{w,sat}$ is the saturated water pressure.

In this model the anodic activation overpotential is assumed to be constant. However, the overpotential at the anode is much smaller than the overpotential at the cathode, and will therefore not be of great importance [15]. Due to current conservation, the average current density at the anode and at the cathode need to be equal. Hence the anodic overpotential can be found by applying an algorithm which calculates the Butler-Volmer equation using a value for the overpotential that gives an average current density at the anode equal to the value found at the cathode.

The total cell potential for the fuel cell is calculated in the post-processing:

$$E^{cell} = E_{cathode} - E_{anode} - \eta_{mem} - \eta_{contact} \quad (2.30)$$

where $E_{cathode}$ is the cathodic half cell potential (reversible cell potential, equation (2.28), minus overpotentials at the cathode), E_{anode} is the anodic half cell potential (reversible cell potential minus overpotentials at the anode), η_{mem} is the potential loss in the membrane, $\eta_{contact}$ is the contact resistance if considered.

Heat sources and sinks

The heat generated in a fuel cell is due to changes of enthalpy and irreversibilities related to charge transfer. In order to calculate the heat generation in each electrode reaction, both charged and non-charged species need to be considered. Values for the entropy of electrons and protons are needed for the computation. In a study by Lampinen and Fomino [23][31] a method of calculating ΔG , ΔH and ΔS for each half-cell reaction is introduced. By calculating the heat generation of each half-cell it is possible to establish how the total heat generation in the fuel cell is distributed between the the cathode and the anode of the cell. This is information that the total reaction of the cell does not give [23]. Due to low conductivity in the membrane, distributed heat sources are important in order to get the right temperature profile in the fuel cell.

The energy balance for a half-cell can be written as [23]:

$$\dot{Q} = r\Delta H + P_{el} \quad (2.31)$$

where \dot{Q} is the heat absorbed, r is the reaction rate of the half cell reaction, ΔH is the half cell reaction enthalpy and P_{el} is the electric power.

It can be shown (See Appendix B) that the heat production/absorption for a real process can be given as [23] [16]:

$$\dot{q} = |i/nF|(\Delta H + (-\Delta G)) - |i||\eta| = |i/nF|(T\Delta S) - |i||\eta| \quad (2.32)$$

in which η is the voltage drop (overpotential) due to ohmic losses and reaction resistance and ΔS is the entropy change for the half cell reaction (See Appendix B). The entropy change at standard state with platinum catalyst can be found to be

$\Delta S = 0.104 J/mol \cdot K$ for the anode side, and $\Delta S = -326.36 J/mol \cdot K$ for the cathode side [23] (In this model the entropy change is assumed to be constant, independent of temperature).

Momentum sinks

Since reactants are consumed at the catalyst layer, a momentum sink has to be implemented. The momentum sink can be expressed as:

$$S_{mom} = \frac{\dot{m}_s v}{V} \quad (2.33)$$

where \dot{m}_s is the rate at which mass is sinked, v is the velocity of the sinked mass and V is the cell volume.

2.3.4 Membrane

The primary purpose of the electrolyte is to transport ions from one electrode to the other. However, the two sides of the fuel cell must also be separated so that the reactants do not come into direct contact with each other, but are forced instead to react electrochemically on the electrode surface. In the case of the Proton Exchange Membrane Fuel Cell (PEMFC, or Polymer Electrolyte Membrane Fuel Cell as it also is called) the electrolyte consists of an acidic polymeric membrane, which functions both as a separator and an electrolyte.

Transport and energy equations

The electro-neutrality is assumed prevail inside the membrane. The proton concentration within the membrane is assumed to be constant and equal to the concentration

of fixed sulfonic acid groups. For a fully humidified membrane this is a good assumption since it is all the same environment. According to Bernardi and Verbrugge [3] the proton concentration can be considered constant, and diffusion is not a mode of proton transport in the membrane.

However, at a later stage, consideration should be given to some of the same approaches which are applied for calculations of charges in semiconductors in order to calculate the concentration of protons in the membrane.

In the membrane, equation (2.8) is used, without any convective terms or source terms, to calculate the heat conduction through the membrane.

The potential profile in the membrane is calculated using the transport equation without the convective terms.

$$-\nabla \cdot (\kappa \nabla \phi) = S_\phi \quad (2.34)$$

where κ and S_ϕ are respectively the ionic conductivity and a source term. ϕ is the potential at each location.

The ionic conductivity is dependant on the water content, λ , in the membrane. For a fully humidified membrane values between 14 and 16.8 are reported [6]. In this model a value of 15 is applied. Springer et al. [6] determined experimentally the following relations for the conductivity ($S \cdot cm^{-1}$) of a Nafion 117 membrane:

$$\kappa_{ref} = 0.005139\lambda - 0.00326 \quad \text{for } \lambda > 1 \quad (2.35)$$

$$\kappa(T_{cell}) = \kappa_{ref} \cdot e^{\left(1268 \left(\frac{1}{303} - \frac{1}{T_{cell}}\right)\right)} \quad (2.36)$$

In this model the resistance is assumed to be constant, due to a fully humidified membrane. This gives a conductivity of $13.375 S \cdot m^{-1}$. It should be noted that

the conductivity of a fully humidified membrane obtained using equation (2.35) and (2.36), are higher than the values presented by Sone et al. [32].

Water transport in the membrane

Since this subject was not discussed in the project [16], it will be looked into in more detail in this section.

The conductivity of the membrane is dependent on its degree of humidification. A fully humidified membrane conducts protons better than one that is only partly humidified. For relative humidity of less than 20% the conductivity in the membrane decrease drastically [32]. However, it is important that the pores in the electrodes are not blocked by excess water expelled from the membrane [15]. In this model the membrane is assumed to be fully humidified and, since this is a one-phase model, flooding is not considered.

During operation, the water molecules are transported through the membrane due to several different mechanisms. Several models have been used in the literature to predict the water flow through the membrane. Most of them are focusing on three mechanisms for the water transport: electro-osmosis, diffusion and convection [9].

The approach used in this model is based on the method used by Janssen [33]. In the work by Janssen, no specific mechanism is used to determine the water transport in the membrane. There can be many contributing factors to the driving force behind water transport. Instead, the model uses fundamental thermodynamics to account for all the different mechanisms taking place.

In the membrane the water transport is related to the proton transport due to the electro-osmotic drag. The transport of protons and water through the membrane

can be expressed as [33]:

$$j = -L_{++} \nabla \phi - L_{+w} \nabla \mu_w \quad (2.37)$$

$$N_w = -L_{w+} \nabla \phi - L_{ww} \nabla \mu_w \quad (2.38)$$

where j is the current density of protons, ϕ is the local potential, μ_w is the local chemical potential of water and the L variables are Onsager coefficients. The physical interpretation of L_{++} is the specific proton conductivity, κ [33]. According to Onsager relations $L_{+w} = L_{w+}$. It can be shown that $L_{w+} = \frac{\xi \kappa}{F}$ [33], in which ξ is the number of water molecules transported with each proton.

In order to provide a physical interpretation of L_{ww} , a short derivation is shown:

$$\begin{aligned} \mu &= \mu^0 + RT \ln c \\ \frac{\partial \mu}{\partial x} &= RT \frac{\partial}{\partial x} \ln c \\ \frac{\partial \mu}{\partial x} &= \frac{RT}{c} \frac{\partial c}{\partial x} \end{aligned}$$

The flux due to the last term in equation (2.38) is:

$$N = -L_{ww} \nabla \mu_w$$

where N is a molar flux.

Inserting for the gradient of the chemical potential in the x direction this gives:

$$N = -L_{ww} \frac{RT}{c} \frac{\partial c}{\partial x}$$

This can be written as:

$$N = D \frac{\partial c}{\partial x}$$

where D is a diffusion coefficient taking account for different transport mechanisms

and c is the concentration of water in the membrane.

However, in this model presented by Janssen [33] equation (2.37) and (2.38) are combined in order to express the water flux in terms of the current density of protons:

$$N_w = t_w j - l_{mem} \nabla \mu_w \quad (2.39)$$

in which

$$t_w = \frac{L_{w+}}{L_{++}} \quad (2.40)$$

$$l_{mem} = L_{ww} - \frac{L_{+w}L_{+w}}{L_{++}} \quad (2.41)$$

The parameter t_w is a measure of the electro-osmotic drag and the term $l_{mem} \nabla \mu_w$ is related to the back transport of water in the membrane. Values for l_{mem} for different membranes are given by Janssen [33]. In this model l_{mem} is assumed to be constant as a first step. This is a adequate assumption for a fully humidified membrane [33].

2.4 Boundary Conditions

To all outer interfaces of the computational domains there need to be applied boundary conditions. Also at many of the internal interfaces boundary conditions need to be applied in order to get physical correct values. The general boundary conditions for this model are given in this chapter.

2.4.1 Inlet conditions

Velocity inlet

At first pressure boundaries were used for the flow channels. This did not allow for direct control over mass flow into the channels. As the model was developed with several distinct domains connected by interfaces, the approach using pressure boundaries did not work. In order to solve this problem and at the same time gain better control over the mass flow, velocity specified inlets were applied. (Mass flow specified inlets would also have been a possibility, but were not chosen due to slower convergence).

At the inlet of the flow channels (at both the cathode and the anode side) the boundary values given are the stoichiometric flow rate, temperature and mass fractions. The stoichiometric flow rate, λ , is a term used to specify the amount of reactant fed to the cell. A stoichiometric rate of 1 is the exact amount of oxygen needed for the reaction, while a rate larger than 1 indicates that cell is fed with more reactants than needed. By specifying the stoichiometric flow rate the respective average velocity at the inlet can be calculated. The mass flow into the fuel cell is determined by the usage of reactants times the stoichiometric flow rate. For the cathode side, this gives

a mass flow of oxygen equal to:

$$\dot{m}_{O_2} = \lambda \cdot \frac{M_{O_2}}{4F} i \quad [kg/s \cdot m^3] \quad (2.42)$$

where M_{O_2} is the molecular weight and F is Faraday's constant. The average velocity at the inlet can be specified in different ways. One approach is to continuously calculate the average velocity from the usage of reactants. The average velocity at the inlet of the flow channel at the cathode side then becomes:

$$\bar{v} = \lambda \cdot \frac{\dot{m}_{O_2}}{\rho y_{O_2} A} \quad [m/s] \quad (2.43)$$

where ρ is the mixture density, y_{O_2} is the mass fraction of oxygen and A is the cross section area of the flow channel.

This approach turned out in some cases to converge slowly, since a reduction in the usage of reactants reduces the velocity and vice versa. Another boundary condition that can be used at the inlet is to keep the average velocity constant. The velocity can then, for example, be calculated using several reference values:

$$\bar{v} = \lambda \cdot \frac{I_{ref}}{nF} \frac{1}{x_{i,ref}} \frac{RT}{p_{ref}} \frac{1}{A} \quad [m/s] \quad (2.44)$$

where I_{ref} is a reference current, n is the number of electrons per mol reaction, $x_{i,ref}$ is the reference mol fraction of the reactant at the inlet, and p_{ref} is the reference pressure at the inlet.

The inlet boundary condition used is dependent on the experimental data available, and will be specified in each case.

However, in order to apply this as a boundary condition a velocity profile needs to be found. For fully developed laminar flow, the velocity in the x -direction is a

function of y and z , $u = u(y, z)$. The velocity is zero in the y and z directions, and the pressure is a function of x , $p = p(x)$. The momentum equation in cartesian coordinates can then be reduced to [25]:

$$-\frac{\partial p}{\partial x} + \mu \left(\frac{\partial^2 u}{\partial y^2} + \frac{\partial^2 u}{\partial z^2} \right) = \text{const.} \quad (2.45)$$

The flow is subject to non-slip conditions on the duct surfaces. This is equivalent to a classic Dirichlet problem [34], which has been determined exactly for many non-circular shapes, including rectangular ducts [35]:

$$u = -\frac{16}{\pi^3} \left(\frac{dp}{dx} \right) \frac{a^2}{\mu} \sum_{n=1,3,\dots}^{\infty} \frac{(-1)^{(n-1)/2}}{n^3} \left(1 - \frac{\cosh(n\pi y/2a)}{\cosh(n\pi b/2a)} \right) \cos \left(\frac{n\pi z}{2a} \right) \quad (2.46)$$

where the pressure gradient $\frac{dp}{dx}$ is given in terms of the mean axial velocity u_m [35]:

$$u_m = -\frac{1}{3} \left(\frac{dp}{dx} \right) \frac{a^2}{\mu} \left(1 - \frac{192}{\pi^5} \left(\frac{a}{b} \right) \sum_{n=1,3,\dots}^{\infty} \frac{1}{n^5} \tanh \left(\frac{n\pi b}{2a} \right) \right) \quad (2.47)$$

where a is the half width of a non-circular duct and b is the half height of a non-circular duct.

Equation (2.46) and (2.47) are fairly complex. In order to circumvent the computational complexity a simple approximation proposed by Purday has been used [35]:

$$u = u_{max} \left(1 - \left(\frac{y}{b} \right)^n \right) \left(1 - \left(\frac{z}{a} \right)^m \right) \quad (2.48)$$

$$u_{max} = u_m \left(\frac{m+1}{m} \right) \left(\frac{n+1}{n} \right) \quad (2.49)$$

where u_m is the average velocity and can be found from equation (2.43) or (2.44).

Relations for the values m and n are [35]:

$$m = 1.7 + 0.5 \cdot \left(\frac{a}{b}\right)^{-1.4}$$

$$n = \begin{cases} 2 & \text{for } \frac{a}{b} \leq \frac{1}{3} \\ 2 + 0.3\left(\frac{a}{b} - \frac{1}{3}\right) & \text{for } \frac{a}{b} \geq \frac{1}{3} \end{cases}$$

which gives velocity profiles that are within 1% of the values obtained from the exact solutions given by equation (2.46) and (2.47). Figure 2.2 shows a plot of a velocity profile using equation (2.48).

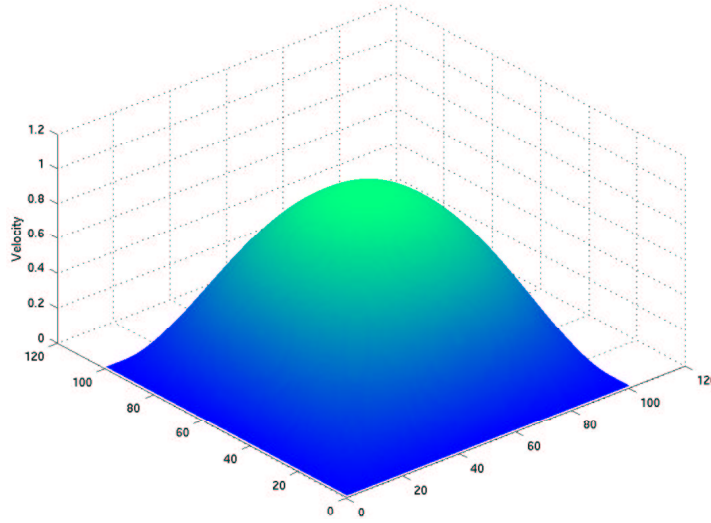


Figure 2.2: Velocity profile for a square channel, $\frac{a}{b} = 1$

The option to have fully humidified flow into the flow-channels is implemented. The saturation pressure for water vapour is given as a quartic equation developed

using a regression of tabulated values from Moran et al. [36].

$$p_{w,sat} = (1.268366 \cdot 10^{-8} \cdot T^4 - 1.498267 \cdot 10^{-5} \cdot T^3 + 0.0067091643 \cdot T^2 - 1.348318703 \cdot T + 102.5034101) \cdot 10^5 \quad [\text{Pa}] \quad (2.50)$$

This equation is valid for temperatures from $323.15K$ to $383.15K$ ($50 - 110^\circ C$).

The mol fraction of the different species at the inlet are given as:

$$\begin{aligned} x_{H_2O} &= \frac{p_{w,sat}}{p} \\ x_{H_2} &= 1.0 \cdot (1 - x_{H_2O}) \\ x_{O_2} &= 0.21 \cdot (1 - x_{H_2O}) \\ x_{N_2} &= 0.79 \cdot (1 - x_{H_2O}) \end{aligned} \quad (2.51)$$

The mass-fraction can then be found by:

$$y_i = \frac{x_i M_i}{\sum_{j=1}^n x_j M_j} \quad (2.52)$$

2.4.2 Outlet conditions

In this model pressure outlets have been used. This is done in order to give the two flow channels a reference pressure at the outlet. Fluent does not have the option to specify two different reference pressures, which is needed in this model since the two channels are separated (see section 2.4.3).

If there is back-flow in any of the two channels, the composition of the flow is calculated as it was for the inlet. This is done only for computational reasons since there should not be any back-flow in the fuel cell under normal operation conditions.

2.4.3 Boundary conditions at internal interfaces

Interface between the electrode and the flow channel

At the interface between the electrode and the flow channel, a user defined function (UDF), which assures that the flux of electrons is zero, is applied. This is done by forcing the value of the potential in the first cell in the flow-channel side of the interface to have the same value as the adjacent cell on the electrode side. By doing that the potential gradient normal to the interface will be zero, hence the flux of electrons is equal to zero.

Interface between the electrode and the membrane

In this model the interface between the membrane and the electrodes is defined as a wall (impermeable boundary). The wall has a fluid region on each side, and each side is therefore treated as a distinct wall. In Fluent this is done by creating a “shadow” of the wall. The “two walls” are thermally coupled. That means the heat transfer will be directly calculated from the solution in the adjacent cells. Therefore, there is no need for any additional boundary conditions [19].

The reason for using a wall at the interface is mainly to prevent any crossover of species and electrons through the membrane and also to prevent pressure related problems. This is done as a first step, and should be investigated further.

The potential in the membrane is set to zero at the anode side, at the interface between the catalyst and the membrane. This is based on the assumption that the potential at the anode side is uniform (see section 2.3.3). At the cathode side, a negative flux equal to the consumption of protons in the adjacent cell in the catalyst layer is specified at the interface between the electrode and the membrane. By doing this, the potential profile in the membrane can be calculated.

As described in section 2.3.4 the gradient of the chemical potential is used to calculate the water flux through the membrane. The profile of the chemical potential in the membrane is computed by specifying the value at the membrane/electrode interface. Local equilibrium is assumed at the interface. This means that at the interface, the water in the membrane and the water vapour in the electrode are in equilibrium. The boundary conditions at the interface at both sides (anode and cathode) can then be given as [33]:

$$\mu_w^{mem} = \mu_w^0 + RT \ln \frac{p_w}{p^\circ} \quad (2.53)$$

where μ_w^{mem} is the chemical potential of water vapour in the membrane at the interface, μ_w^0 is the chemical potential at standard conditions, p_w is the water vapour pressure in the electrode at the interface, and p° is the standard pressure.

2.4.4 Land areas

In the areas where the gas diffusion electrodes are connected to the bipolar plates (the land area) a constant reference voltage equal to zero is applied as a boundary condition both at the anode and at the cathode. At all the other walls the electron flux is set to zero.

2.4.5 Walls

On all walls the no-slip boundary condition is applied, for the momentum equations.

Different boundary conditions for the energy equation can be employed in this model. Specified heat flux, temperature or convective heat transfer can be applied. The boundary condition used will be specified for every case presented in this thesis.

Fluent does not solve user-defined scalars in solid regions, so potential profiles are not calculated in the bipolar plates.

2.5 Computational Procedure

In this model, the segregated implicit solver has been used. In a segregated solver the governing equations are solved sequentially (segregated from one another). The governing equations are non-linear (and coupled), therefore several iterations of the solution loop must be performed before a converged solution is obtained. Each iteration consists of the steps illustrated in figure 2.3 [19][24]. It should be noted that using residual values in order to determine convergence is not sufficient. The values of critical parameters should be monitored in order to secure convergence.

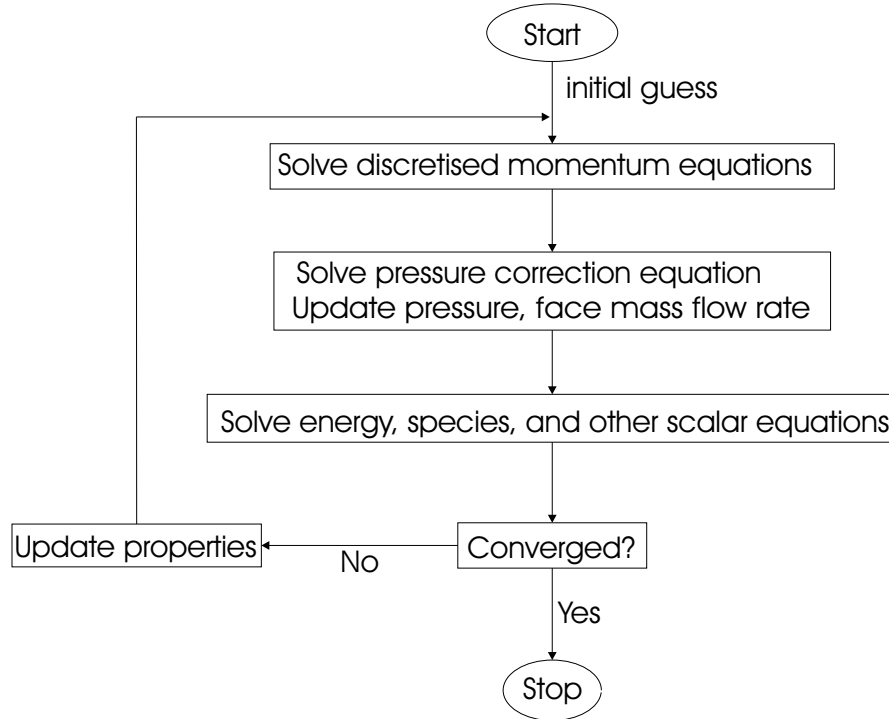


Figure 2.3: Solver algorithm

A finite volume method is used to solve the coupled system of partial differential equations, which are subject to several boundary conditions. The finite volume method reduces the set of differential equations into a system of algebraic equations corresponding to the nodes of the computational mesh. The key step of the finite volume method is the integration of the governing equations over a control volume to yield discretized equations. This gives, for a control volume the steady state general transport equation [24]:

$$\oint \rho \phi \vec{v} \cdot d\vec{A} - \oint \Gamma_\phi \nabla \phi \cdot d\vec{A} - \int_V S_\phi dV = 0 \quad (2.54)$$

For flux in x-direction this gives:

$$(\rho \phi v A)_e - (\rho \phi v A)_w - \left(\left(\Gamma_\phi A \frac{\partial \phi}{\partial x} \right)_e - \left(\Gamma_\phi A \frac{\partial \phi}{\partial x} \right)_w \right) - \bar{S}_\phi \Delta V = 0 \quad (2.55)$$

in which ϕ is a general variable, Γ_ϕ is diffusion coefficient for ϕ , ΔV is the volume and \bar{S}_ϕ is the average value of the source of ϕ over the control volume. The subscript e and w indicates that the values are taken respectively at the eastern or western control volume face.

There are different ways of approximating the values at the control volume faces. The following discretisation schemes have been applied for solving the scalars:

Scalar	Scheme
Pressure	“Standard”
Momentum	Second order upwind
Energy	Second order upwind
Concentrations	Second order upwind
Potential	Second order upwind
Chemical potential	Second order upwind

Table 2.1: Discretisation schemes for the scalars used in this model

The “Standard” scheme for pressure discretisation is the default in FLUENT. This discretisation interpolates the pressure values at the faces using momentum equation coefficients. This procedure is viable as long as the pressure variation between cell centres is smooth [19].

It should be noted, that the diffusion terms are central-differenced and are always second-order accurate [19].

The pressure has been coupled with the velocity using the SIMPLE algorithm. SIMPLE stands for Semi-Implicit Method for Pressure-Linked Equations. The SIMPLE algorithm is a prediction-correction procedure for calculation of pressure using corrected velocities [24].

Fluent modelling capabilities cover a broad range of thermo-fluid phenomena, but no modelling capabilities for physico-chemical transport in fuel cells. The model equations specific to fuel cells (section 2.3.3 and 2.3.4) as well as the voltage-current algorithm were implemented by developing a set of User Defined Functions (UDFs). UDFs can be dynamically linked with the Fluent solver to enhance and customise the standard features of the code. User-defined functions are written in the C programming language. Standard C library functions can be used in user-defined functions. There are also predefined macros available, that are provided by Fluent Inc., which allow access to data in the Fluent solver. The user-defined functions have been implemented as compiled functions, which means that they are linked with the standard executable file in Fluent [19].

2.5.1 Parallel solver

Due to the complexity of the physics in a fuel cell, a large number of computational cells needs to be used for proper resolution. A parallel solver makes it possible to use

multiple processes while computing a solution, and thereby reduces the computing time. Fortunately FLUENT has both a serial and a parallel solver.

Care must be taken while writing user defined functions for a parallel solver. The user defined functions for this model have been written in such a way that they can be used in both parallel and serial modes. Tests have been performed in order to make sure that the two modes yield same results.

The parallel solver splits up the geometry into multiple partitions or domains. Each partition is assigned to a different CPU (or node). This means that the number of partitions is an integral multiple of the number of computer nodes available.

“Parallel processing in FLUENT involves an interaction between FLUENT, a host process, and a set of compute-node processes. FLUENT interacts with the host process and the collection of compute nodes using a utility called cortex that manages FLUENT’s user interface and basic graphical functions.” [19]

FLUENT uses a host process that distributes commands to the other compute nodes via a socket communicator to a single designated compute node called compute-node-0. The host node does not contain any grid data and therefore uses a minimal amount of resources. Compute-node-0 distributes the host commands to the other compute nodes. Communication from the compute nodes to the host is only possible through compute-node-0. This communication can only occur when all compute nodes have been synchronised with each other. Each compute node simultaneously executes the same program on its own data set. The parallel architecture which is used in FLUENT is shown in figure 2.4 [19].

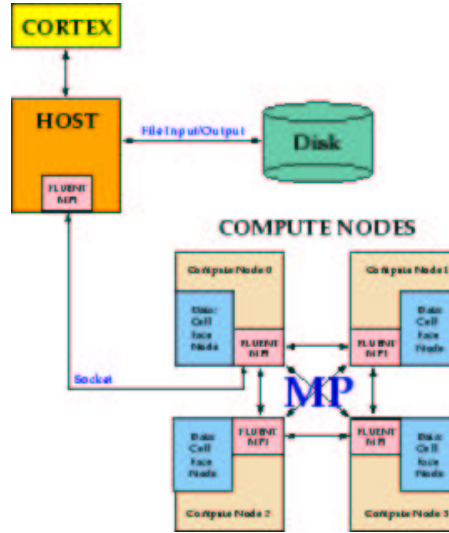


Figure 2.4: FLUENT parallel architecture [19]

2.6 Summary

In this chapter, the theory that describes the physics occurring within in a proton exchange membrane fuel cell (PEMFC) has been presented. A one-phase, three-dimensional, non-isothermal model with variable overpotential at the cathode catalyst layer was described. The equations and the boundary conditions used in this model were presented. The model is based on several assumptions which were presented in this chapter. The methodology used by the CFD code, to solve the problem, was also briefly described.

Chapter 3

Straight Channel Test Case

This chapter describes a straight channel fuel cell model. The parameters and operation conditions applied are similar to the ones used by L. Wang et al. [22]. Wang et al. present both experimental data for a single PEM fuel cell and results obtained from a 3-D model. Since the model presented in this thesis only is a one-phase model and this case only consider a straight channel, the same results are not expected.

To verify a fuel cell model is not very easy. Benchmarks with detailed data do not exist. It is usual to compare results from the model with polarisation curves obtained from experiments or other models. This is not a very satisfactory way of verifying the model, even one-dimensional models can fit a polarisation curve. However, most publications uses only a comparison of polarisation curve obtained from the model with data obtained from experiments. Since measuring values and profiles inside the fuel cell is difficult without interfering with the processes, it is hardly possible to obtain data that can be used to verify the model. Due to lack of any better way of verifying the model, polarisation curves will be used. However, analysis of the physical results given by the model will be preformed.

What is more important than the actual values that the model is providing, is the trends which it is describing. Even though the absolute values may be inaccurate due to incorrect parameters, the physics implemented in the model should be correct and therefore the predicted trends should be physically representative. This can give us vital information of how the fuel cell is behaving, and provide a basis for design optimisation.

It should also be emphasised that the mass, species and energy balances are monitored in order to ensure global conservation of the mass and energy.

3.1 Modelling Parameters

One of the tedious parts of modelling is the determination of the parameters for the model. The accuracy of the parameters will in the end be one of the determining factors for the accuracy of the results.

Table 3.1 shows the dimensions of the computation domain used in this straight channel case [22].

Parameter	Value	Unit
Cell width	$2.0 \cdot 10^{-3}$	m
Channel length	0.07	m
Channel height	$1.0 \cdot 10^{-3}$	m
Channel width	$1.0 \cdot 10^{-3}$	m
Land area width	$1.0 \cdot 10^{-3}$	m
Electrode thickness	$0.3 \cdot 10^{-3}$	m
Catalyst layer thickness	$1.29 \cdot 10^{-5}$	m
Membrane thickness	$0.108 \cdot 10^{-3}$	m

Table 3.1: Physical dimensions for the straight channel case

A cross-section of the computational grid that is used in the straight channel case is shown in figure 3.1. The geometry of the fuel cell simulated in this work consists of

bipolar plates and two flow channels separated by anodic and cathodic diffusion layers and the membrane. Both the anode and the cathode flow channel are divided into $20 \times 18 \times 150$ grid cells. The membrane is simulated with $40 \times 7 \times 150$ computational cells. Both gas diffusion layers are divided into $40 \times 12 \times 150$ cells. The catalyst layers are divided into $40 \times 1 \times 150$ cell each. The total number of grid cells used, including the bipolar plates, is 546000. It should be noted that this is a much finer grid than e.g. what Shimpalee et al. [11][37][38] are using in their studies (See section 3.2 for a grid study of the fuel cell channel used in this study), and this fine resolution is made possible by use of a parallel solver

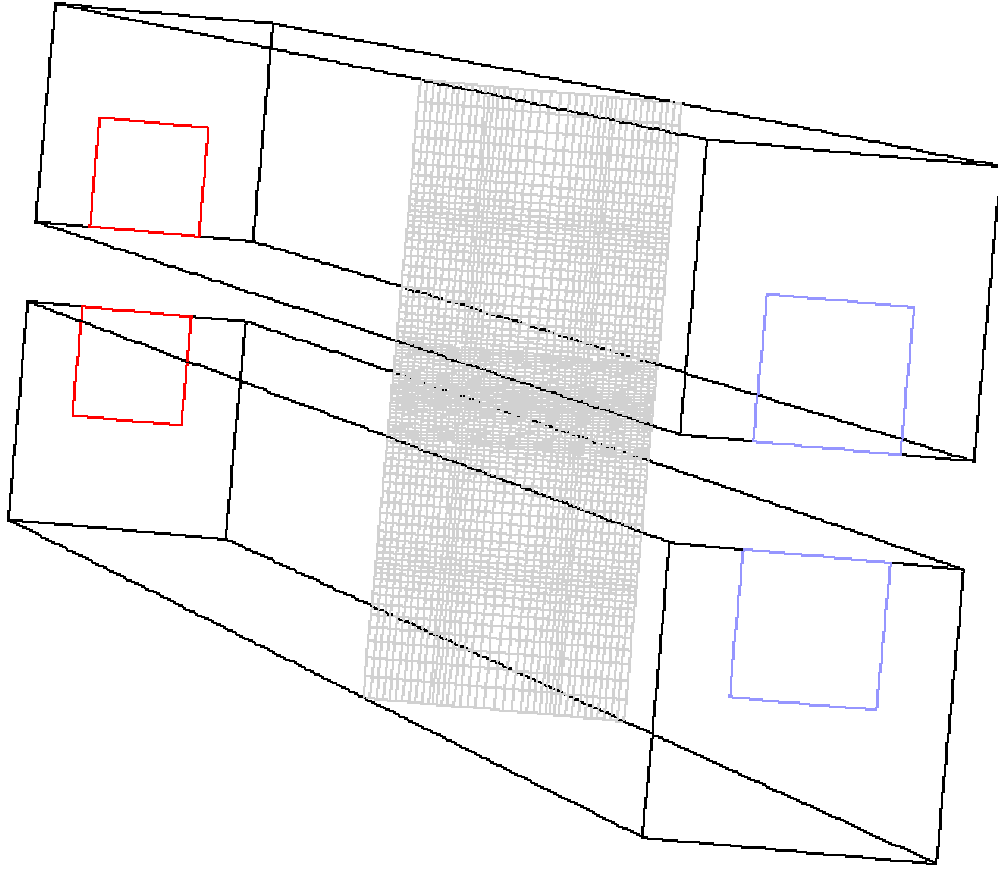


Figure 3.1: Cross-section of the computational grid

Table 3.2 gives the basic operating conditions for the fuel cell [22]. Since this case does not include a serpentine flow channel, but only one single channel length, the mass flow rate given by L. Wang et al. [22] can not be used. Instead, a flow rate corresponding to a stoichiometry of 3 is applied.

Parameter	Value	Unit
Inlet temperature, anode and cathode	80	$^{\circ}C$
Anode side pressure	3	atm
Cathode side pressure	3	atm
Anode stoichiometric flow rate	3	-
Cathode stoichiometric flow rate	3	-
Relative humidity of inlet gases	100	%
Oxygen/Nitrogen ratio	0.79/0.21	-

Table 3.2: Operation parameters for the straight channel case

In this straight channel case the velocity inlet boundary condition described in equation (2.42) and (2.43), in which the inlet velocity is calculated as a function of the actual consumption of reactants, is used.

The reactants are assumed to be fully humidified at the inlets. The humidification temperature is set equal to the cell temperature, $80^{\circ}C$ [22]. In this case the mass fraction at the inlets are assumed to be constant.

Specie	Mass fraction, %
H_2O , anode	62.253
H_2 , anode	37.747
H_2O , cathode	10.344
O_2 , cathode	20.885
N_2 , cathode	68.771

Table 3.3: Mass fraction at the inlets, fully humidified flow

The single phase assumption implies that the product water is in the gas phase, hence since the inlet flow is fully humidified the relative humidity is expected to exceed 100%.

Parameter	Symbols	Value	Unit	Ref.
Electrode porosity	γ	0.4	-	[22]
Permeability	α	$1.76 \cdot 10^{-11}$	m^2	[22]
Thermal conductivity:				
solid region	k	150.6	$W/(m \cdot K)$	[2]
Electronic conductivity	σ	100	S/m	[39]
Asymmetry parameter:				
Anode	β	0.5	-	[29][40]
Cathode	β	1.0/0.5	-	[4][40][29][41]
Concentration parameter:				
Hydrogen	γ_{H_2}	0.25	-	[4]
Oxygen	γ_{O_2}	0.5	-	[4]
Constant, anode	k_a	$17.00 \cdot 10^7$	-	-
Constant, cathode $\beta = 1.0$	k_c	$40.75 \cdot 10^{-11}$	-	-
Constant, cathode $\beta = 0.5$	k_c	0.8093958	-	-

Table 3.4: Electrode properties for the straight channel case

The gas diffusion and catalyst layer properties used in most of the simulations are given in Table 3.4. In the literature different names and values are used for the asymmetry parameter, also called transfer coefficient. The value of β ranges from 1 to 0 [41]. Because of the inconsistency in the literature a parametric study of the asymmetry parameter at the cathode has been preformed. Simulations with an asymmetry parameter equal to 1 and 0.5 have been conducted (see section 4.1 and 4.6).

It should be noted that the value given by Bernardi and Verbrugge [4] for the transfer coefficients at the anode, is not strictly consistent with the Butler-Volmer equation [29][41] which require that the coefficients for the forward and backward component of the equation should add to unity. The values for transfer coefficients at the anode given by Bernardi et al. [4], which also was used by L. Wang et al. [22], is therefore not used in this model. However, the activation overpotential at the anode is much smaller than the activation overpotential at the cathode. Which means, that

the value of the charge transfer coefficients at the anode is of less importance.

The permeability to hydrogen in the gas diffusion layer is assumed to be equal to the permeability to air in the gas diffusion layer. The value for the permeability to air is given by L. Wang et al. [22].

In this case the volume fraction of membrane in the catalyst layer is not taken into account.

The constants k_a and k_c are dependent on the geometry of the catalyst layer (catalyst loading etc.) and are specified to fit the polarisation curve for one voltage value, then they are kept constant for the rest of the simulations. In order to calculate k_a , it is assumed that the activation overpotential at the anode is about an order of magnitude less than the activation overpotential at the cathode at current densities about $0.3A/cm^2$. In this model, the average current density at the anode and the cathode are considered to be equal when the difference is less than $2000A/m^3$, which corresponds to a value of $2.58 \cdot 10^{-6}A/cm^2$. This is a very small difference that in most cases can be neglected.

Table 3.5 lists the membrane properties for the straight channel case. It should be

Parameter	Symbols	Value	Unit	Ref.
Thermal conductivity	k	0.67	$W/(m \cdot K)$	[2]
Proton conductivity	κ	13.375	S/m	[6]
Permeability in the membrane	l_{mem}	$2.35 \cdot 10^{-7}$	$mol^2 \cdot s/(m^3 \cdot kg)$	[33]
Fixed-charge concentration	-	1200	mol/m^3	[4]
Number of water molecules transported per proton	ξ	3	-	[33][32]

Table 3.5: Membrane properties for the straight channel case

noted that the fuel cell used by L. Wang et al. [22] contains a Nafion 115 membrane, while the proton conductivity is based on a study of a Nafion 117 membrane [6] and the value for the permeability in the membrane is based on a Nafion 112 membrane

[33]. The number of water molecules transported per proton is assumed to be constant in this model.

Constant temperature boundary conditions were applied to the outer walls of the fuel cell. The fuel cell temperature is maintained at 80°C in the straight channel case. The thermal conductivity of the bipolar plates is set to $35\text{W}/(\text{m} \cdot \text{K})$ and the electrical resistance is set to $50 \cdot 10^{-6}\Omega \cdot \text{m}$, which are a mid-range values of data presented by Middelmann et al. [42]. The electrical contact resistance is set to zero in this case. In the experiments conducted by L. Wang et al [22] gold-plated copper plate were used to connect the bipolar-plates with the external circuit.

All other properties used for the fluids and solids are taken from Mills [18] and are given in Appendix C for completeness.

3.2 Grid Study

For laminar flow in ducts with rectangular cross section, the wall friction will vary greatly, being largest near the midpoints of the sides and near zero in the corners. The viscous boundary layers will grow downstream, retarding the axial flow at the wall and thereby accelerating the flow in the centre-core in order to maintain the incompressible continuity [25]. This makes it necessary to have a denser grid near the walls to capture the large change in the velocity gradient, due to the non-slip condition at the walls. It is also desirable to have a sufficiently dense grid near the porous media, to capture the flow field. To achieve a good current density profile and a correct overpotential distribution in the catalyst layer, a finer grid is also needed in this area of the fuel cell.

However, to reduce the computation time, it is very important to decrease the number of computation elements, but at the same time keep sufficient accuracy. In

order to find a reasonable number of cells, that still achieve good physical results, a grid study has been preformed.

The preprocessor used in this study was Gambit 2.0. Fluent 6.1 uses unstructured grids, and does not support a structured grid.

The geometry of the fuel cell simulated in this work consists of two flow channels separated by anodic and cathodic diffusion layer and the membrane. In the base case (grid A) both the anode and the cathode flow channel was divided into $20 \times 18 \times 150$ grid cells. The membrane was simulated with $40 \times 7 \times 150$ grid cells. Both gas diffusion layers was divided into $40 \times 12 \times 150$ grid cells. The catalyst layers were simulated divided into $40 \times 1 \times 150$ grid cell each. The total number of grid cells used, including the bipolar plates, was 546000. Such a fine grid was used, in order to make sure that all the transport mechanisms in the fuel cell was properly captured.

For the grid study, two meshes with respectively 155925 (grid B) and 66240 (grid C) computational cells each was created. It should be noted that more important than the total number of cells used in the mesh is the distribution of the cell elements. Table 3.6 shows how the computational cells are distributed in the three different grids used in this study.

	Grid A	Grid B	Grid C
Flow channel	$2 \times (20 \times 18 \times 150)$	$2 \times (13 \times 10 \times 105)$	$2 \times (11 \times 9 \times 60)$
Gas diffusion layer	$2 \times (40 \times 12 \times 150)$	$2 \times (27 \times 9 \times 105)$	$2 \times (23 \times 7 \times 60)$
Catalyst	$2 \times (40 \times 1 \times 150)$	$2 \times (27 \times 1 \times 105)$	$2 \times (23 \times 1 \times 60)$
Membrane	$40 \times 7 \times 150$	$27 \times 5 \times 105$	$23 \times 4 \times 60$
Bipolar plate	2×126000	2×48720	2×13380
Total	546000	155925	66240

Table 3.6: Computational grid parameters

At cathode voltage of 15.444V, the coarsest grid having 66240 computational cells (grid C) shows a deviation of less than 1.2% for the average current density from the

case with 546000 cells. The grid with 155925 cells (grid B) deviates by about 0.9% for the average current density. These are small deviations, however, it is necessary to see the result of the lower resolution in the catalyst layer. This could significantly affect the current density profiles which are of particular interest in this study. In order to investigate this, a plot of the deviation in the local current density between grid A (546000 computational cells) and the two coarser grids has been made. Figure 3.2 and 3.3 shows that the relative difference in the local current density is increasing along the channel. It can be seen that grid B (155925 cells) provides a more accurate solution than grid C (66240 computational cells). However, both the grids are giving reasonable results for this straight channel case with developed flow at the inlets. It should be noted that if a longer channel or a flow channel with bends is applied, the deviation might be of larger importance for the coarsest grid. A similar study should be performed for each geometry.

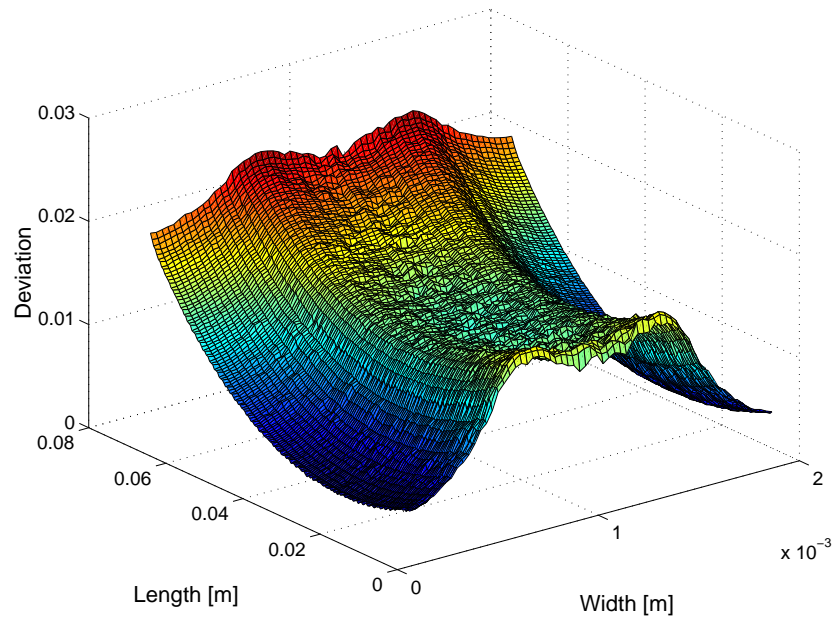


Figure 3.2: Relative difference in the local current density between grids C and A (Reference grid A)

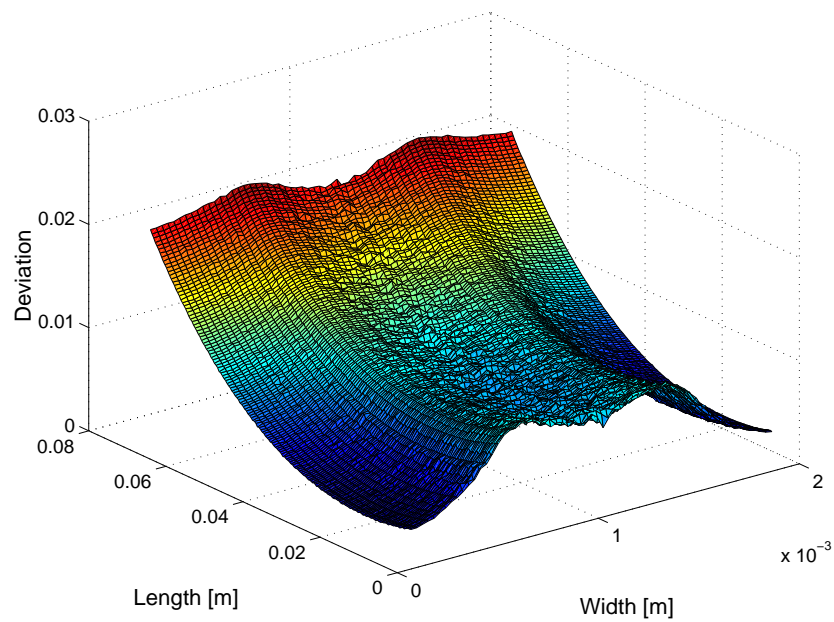


Figure 3.3: Relative difference in the local current density between grids B and A (Reference grid A)

Chapter 4

Results and Discussion

The results obtained for the straight channel case is presented and discussed in this section. All the computations were performed on a Linux computer cluster with dual 2000+ AMD Athlon processors on each node. The maximum number of processors used were eight. The number of iterations required and the computation time was dependent of the initial conditions specified and the input of the cathode half cell voltage. At very low current densities the rate of convergence is very low, so full convergence requires very lengthy computational time.

4.1 Polarisation Curve

As discussed earlier good agreement between measured and computed polarisation curves is not sufficient to determine whether the model is correct or not, but a correct model should be able to fit the polarisation curve. In order to see how the asymmetry parameter affects the polarisation curve, simulations have been performed with two different values for the asymmetry parameter, $\beta = 1.0$ and $\beta = 0.5$. Figure 4.1 show

the polarisation curves obtained by the model compared with experimental results reported by L. Wang et al. [22]. The values given by the model are also presented in Table 4.1 and 4.2.

Cathode voltage, V_{ref} [V]	Current densities [A/cm^2]	Voltage [V]
15.500	0.0010430	0.910116
15.480	0.0098140	0.888102
15.460	0.0686525	0.854785
15.444	0.2686159	0.797982
15.430	0.5861942	0.732153
15.420	0.8659466	0.683230
15.410	1.1679290	0.634474
15.405	1.3246585	0.610223
15.395	1.5785960	0.569816
15.389	1.8480318	0.532415

Table 4.1: Polarisation data provided by the model, $\beta = 1$

Cathode voltage, V_{ref} [V]	Current densities [A/cm^2]	Voltage [V]
15.500	0.0102785	0.907639
15.480	0.0371641	0.881601
15.455	0.1579754	0.830593
15.444	0.2691073	0.797886
15.425	0.5567812	0.733262
15.405	0.9886427	0.652195
15.390	1.3662734	0.590147
15.385	1.4821476	0.574164

Table 4.2: Polarisation data provided by the model, $\beta = 0.5$

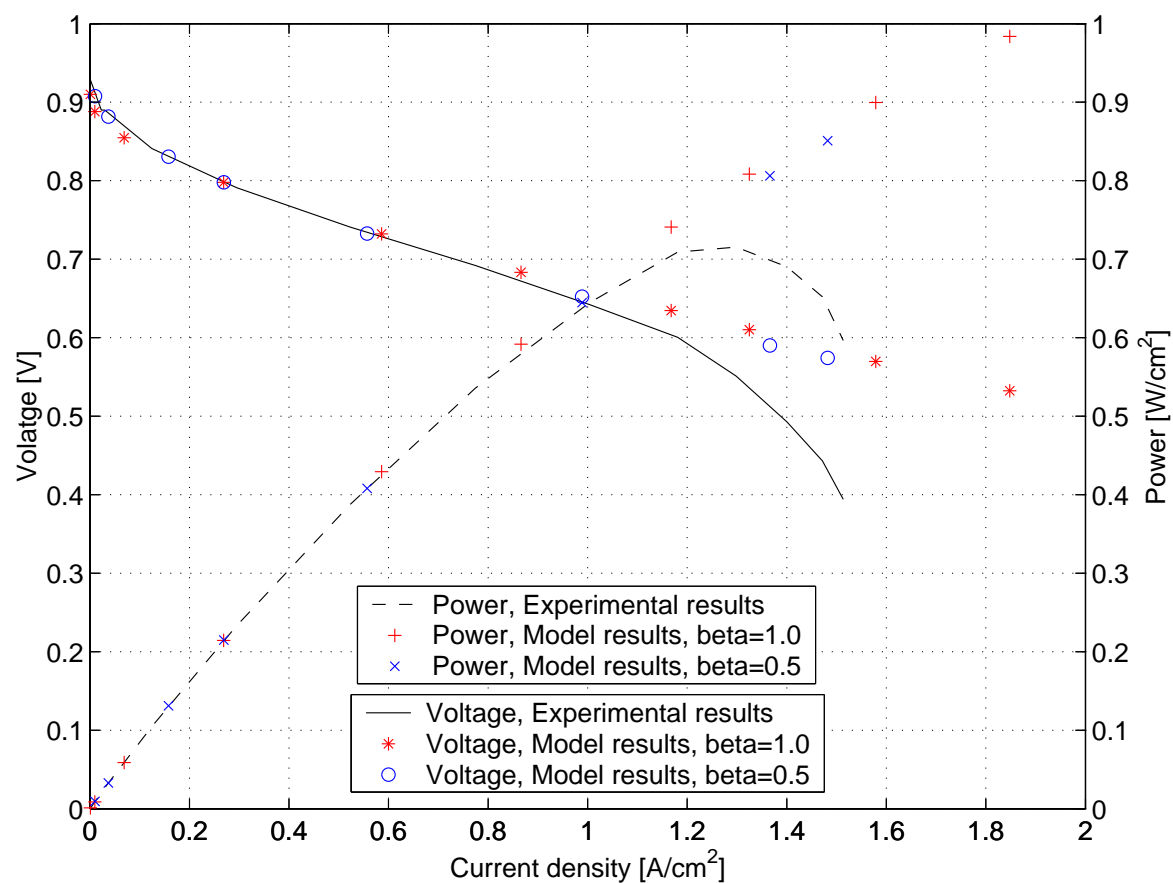


Figure 4.1: Polarisation curve

For low and mid-range current densities, often respectively referred to as the activation and the ohmic region of the polarisation curve, the results from the model correspond well with the experimental results. The deviation in this regions are less than 5.0% for $\beta = 1.0$ and less than 1.1% with $\beta = 0.5$. These results are very good considering the restrictions of this model, and the fact that not all the parameters used are taken from the actual fuel cell used in the experiments.

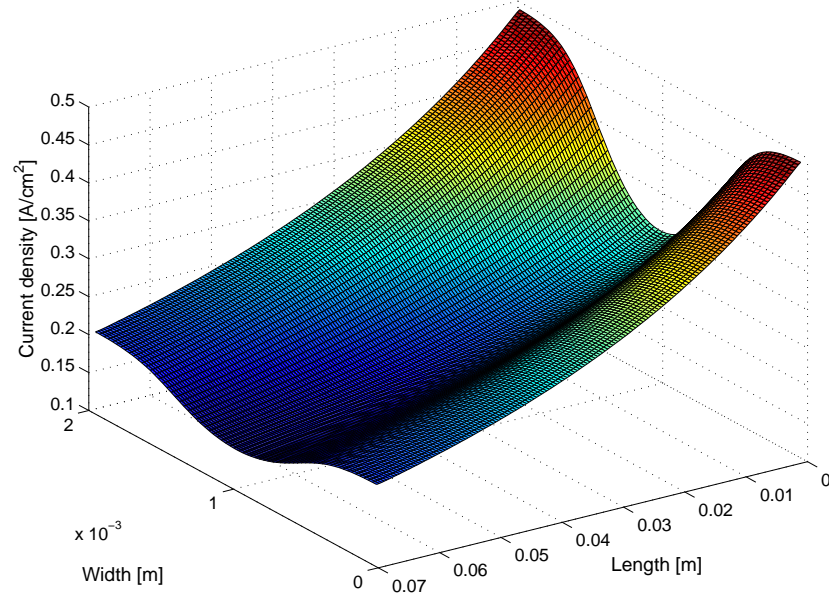
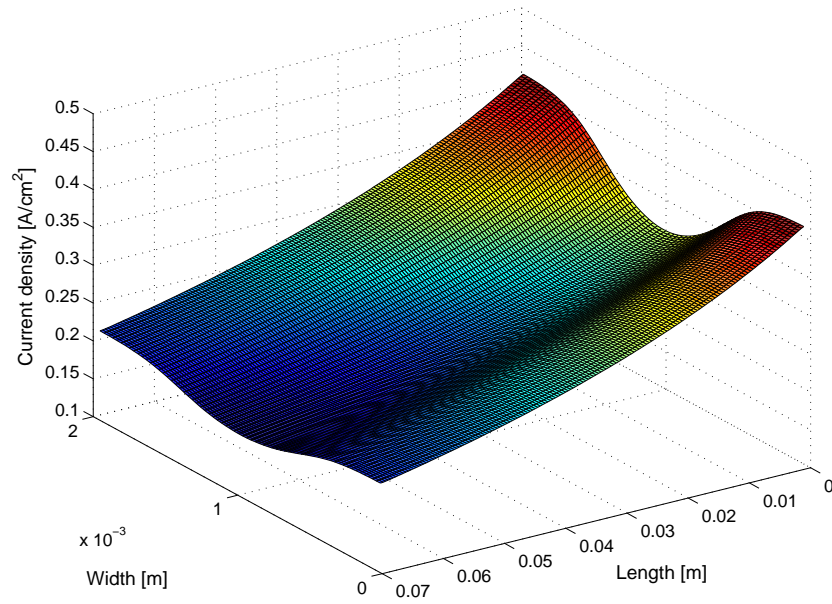
Especially at very low average current densities the simulations with $\beta = 0.5$ shows better ability to follow the experimental results than the simulations with $\beta = 1.0$. This suggests that the actual value of the asymmetry parameter should be closer to 0.5 than 1.0. This is in accordance with the range of values for the asymmetry parameter presented by Hamann et al. [29].

As expected, the model is not able to follow the experimental values at high current densities. This region of the polarisation curve is often referred to as the mass transport controlled region, because the transport of reactants to the catalyst layer is the dominant limitation to the reaction rate. The deviation between the experimental results and the results obtained by the model can partly be explained by the assumption of a single phase model. At higher current densities there is a high water production at the cathode. The water vapour will exceed the saturation pressure and liquid water will be formed in the gas diffusion layer [2][43]. This will limit the diffusion of oxygen in to the catalyst layer, and thereby increase the overpotential due to mass transport limitations. This explains why the experimental results are decreasing steeply at higher current density, while the one phase model where no liquid water is blocking the diffusion continues on the same slope. Another effect that will lead to a drop in the cell voltage at higher current densities, is that the reaction zone in the catalyst layer tends to move away from the “membrane interface” at higher currents [44]. The protons need to be transported further out in the catalyst layer due to

depletion of oxygen in the catalyst, which will lead to increased ohmic losses. This effect is not taken into account either, since the catalyst is modelled as a single layer of computational cells in this model.

Figures 4.2 and 4.3 show the local current distribution in the cathode catalyst at an average current density of $0.269 A/cm^2$ with an asymmetry parameter of $\beta = 1.0$ and $\beta = 0.5$ respectively. Figure 4.4 shows the relative difference between Figure 4.2 and 4.3. The difference in the current density profiles can be explained by looking at a plot of the current density as a function of the overpotential. As shown in Figure 4.5 the current density is higher at the same activation overpotential with a higher asymmetry parameter, and therefore the current density profile will have larger maxima. Since the average current density is the same in both Figure 4.2 and 4.3, the total oxygen consumption is also the same. Figure 4.2 shows a higher current density at the inlet due to higher asymmetry parameter, and therefore corresponds to a higher oxygen consumption near the inlet. The exchange current density is dependent on the oxygen concentration, and is therefore lower at the outlet for $\beta = 1.0$ (Figure 4.2) than for $\beta = 0.5$ (Figure 4.3). Hence, the local current density is slightly higher closer to the outlet in Figure 4.3 than in Figure 4.2. This shows that a lower value of the asymmetry parameter tends to smooth out the current density profile.

Even though the average current density, the cathode half cell voltage and the cell voltage are virtually identical (maximum deviation less than 0.2%), the difference in the local current density is greater than 18% at some locations (see Figure 4.4). This indicates that the asymmetry parameter is important for the current density distribution. The result is also very interesting because it demonstrates that even though the results fit the polarisation curve, different distributions can be obtained. The non-uniformity can have a significant impact on the design and longevity of a fuel cell.

Figure 4.2: Cathodic current density, $\beta = 1.0$ Figure 4.3: Cathodic current density, $\beta = 0.5$

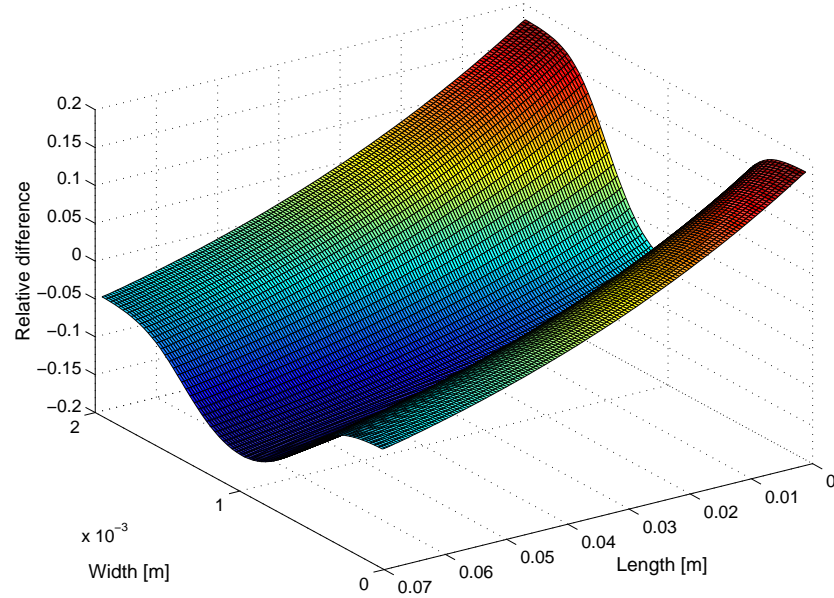


Figure 4.4: Relative difference between the current density profiles with $\beta = 1.0$ and $\beta = 0.5$ (Reference $\beta = 0.5$)

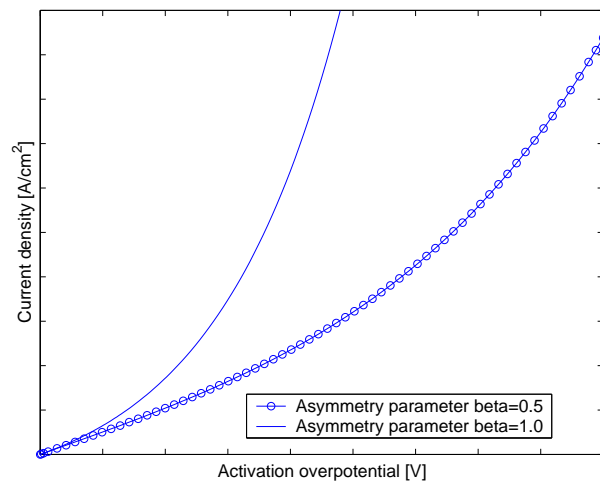


Figure 4.5: Graphical representation of the Butler-Volmer equation, with different asymmetry parameters

4.2 Velocity Contours

Prior to analysing the current density distributions, it is useful to examine the bulk transport in the flow channels and electrodes.

As mentioned earlier a flow rate corresponding to a stoichiometry of three was applied. Figure 4.6 shows the velocity contour in the two channels at different cross-section at an average current density of $0.989 A/cm^2$. The velocity in the cathode flow channel is higher than the velocity in the anode flow channel. The velocity is higher at the cathode side due to lower concentration of oxygen in the mixture. The velocity profile applied as a boundary condition at the inlets, are fully developed and changes very little down the channel.

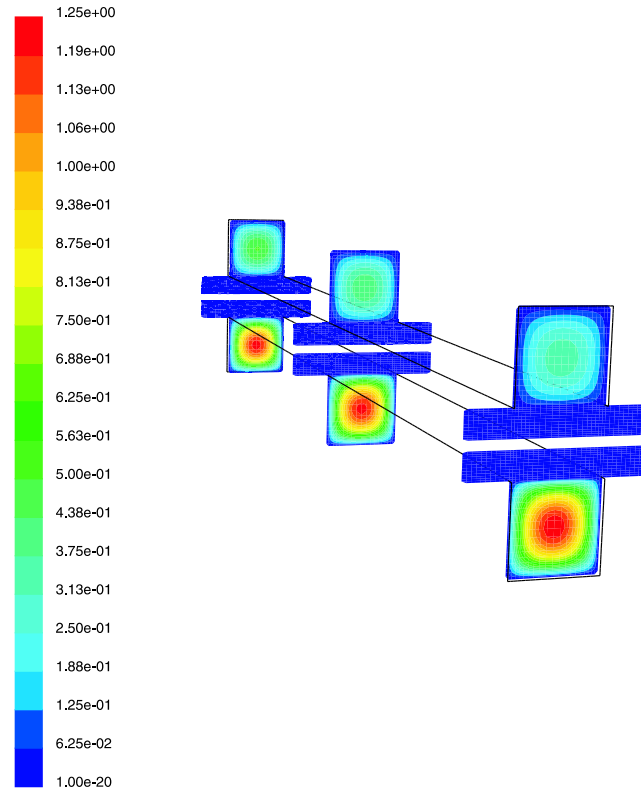


Figure 4.6: Velocity profiles $0.989A/cm^2$, $\beta = 0.5$ (outlet in foreground)

4.3 Concentrations of Reactants

The simulated mass fractions of oxygen and hydrogen are shown for different cross-sections at an average current density of $0.2691 A/cm^2$ in Figure 4.7 and 4.8 respectively. It can be seen that the gradients are much more significant in the oxygen-reduction reaction (cathode side) in comparison with the hydrogen oxidation reaction (anode side). This is in line with what has been predicted by several others [2][12][17][45][44], and is consistent with the mass transport limitations associated with the cathode.

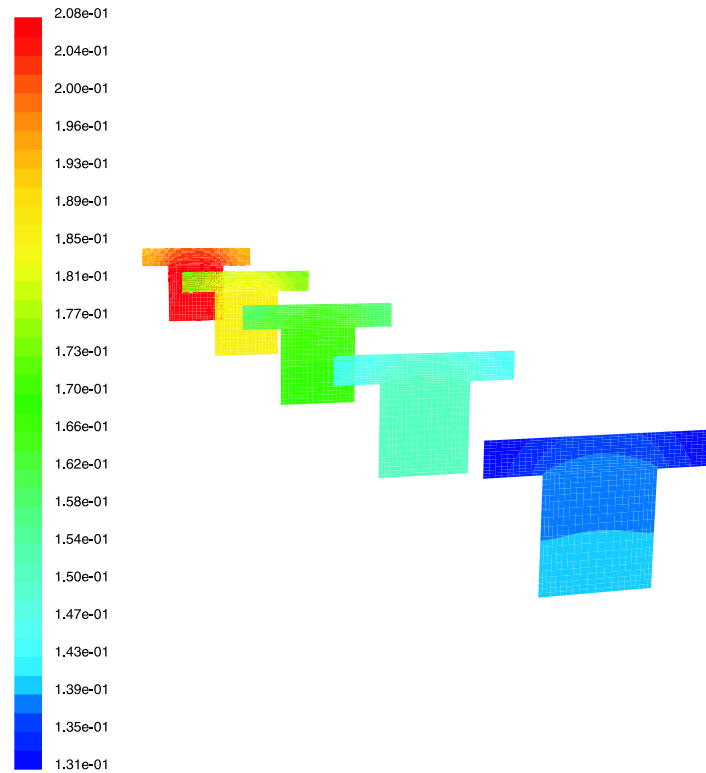


Figure 4.7: Mass fractions of oxygen, $0.2691A/cm^2$, $\beta = 0.5$ (outlet in foreground)

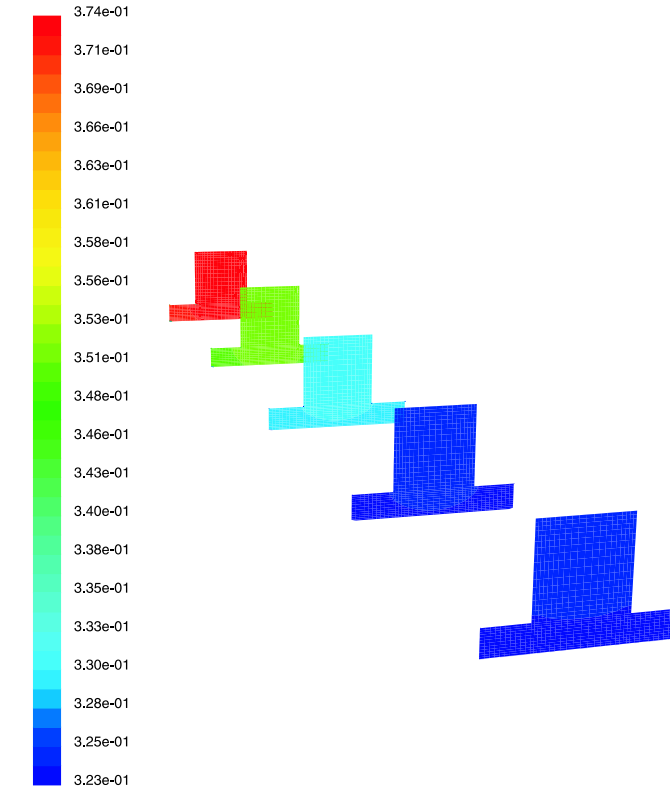


Figure 4.8: Mass fractions of hydrogen, $0.2691A/cm^2$, $\beta = 0.5$ (outlet in foreground)

4.4 Temperature Distribution

Due to time limitations, the effect of the heat generated in the cell has not been investigated in details. However, a brief investigation of the energy boundary conditions has been preformed.

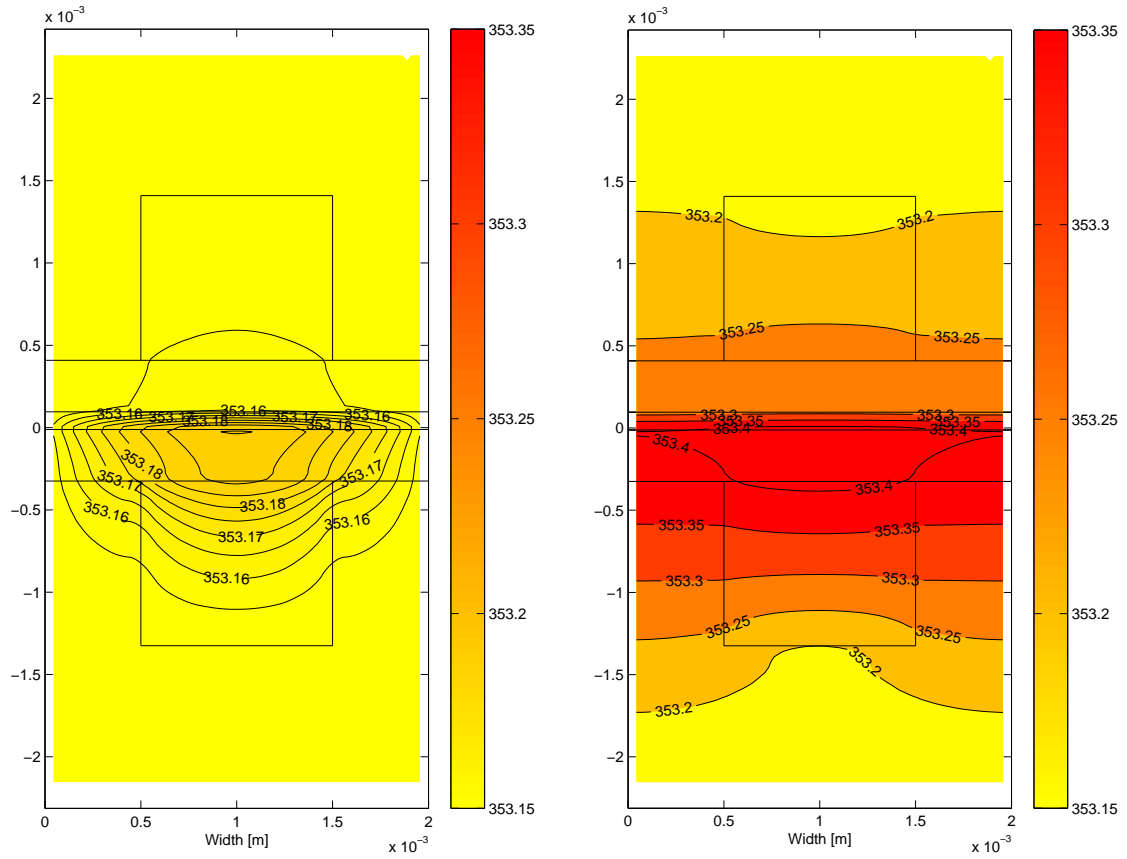
Figure 4.9(a) and 4.9(b) shows the temperature distribution in a cross-section at a cathodic half cell voltage of $15.425V$, using two different energy boundaries. Figure 4.9(a) has constant temperature boundaries, $T = 353.15K$, at all walls. Figure 4.9(b) shows a contour plot with zero energy flux boundaries at the side walls and constant temperature boundaries, $T = 353.15K$, at the top and end walls. (The cathode side is at the bottom in both figures and the boundaries between the flow channels, gas diffusion electrodes, membrane and the bipolar-plate are shown in the figures).

Both figures shows that the the temperature is highest at the cathode catalyst. The heat generation at the anode is very small compared to the heat generation at the cathode side. Due to higher thermal conductivity of hydrogen than of nitrogen or oxygen, the temperature profile is more uniform on the anode side.

Though the temperature profiles are very different in the two figures, it should be pointed out that the maximum temperature difference across the section are of order $0.1^{\circ}K$ and $0.4^{\circ}K$. As expected the temperature profile is much more uniform in the case with constant temperature boundaries. In order to see how the temperature profiles affect the local current distribution in the fuel cell, the relative difference between the two current density profiles is shown in Figure 4.10. Average current density is deviating by less than 0.4%, and it can be seen that the local difference is less than 0.5%. Though the small differences have little impact on the local current density distribution under the conditions investigated here, it should be noted that the temperature profile is expected to have a larger impact when two-phase flow is

considered.

For further studies, better data for the thermal conductivity in the membrane should be obtained and the thermal boundary conditions should be investigated further.



(a) Constant temperature boundaries

(b) Zero flux boundaries at the side walls, constant temperature boundaries at the top and bottom wall

Figure 4.9: Temperature profiles in a cross-section of the fuel cell with two different boundary conditions (top channel corresponds to anode)

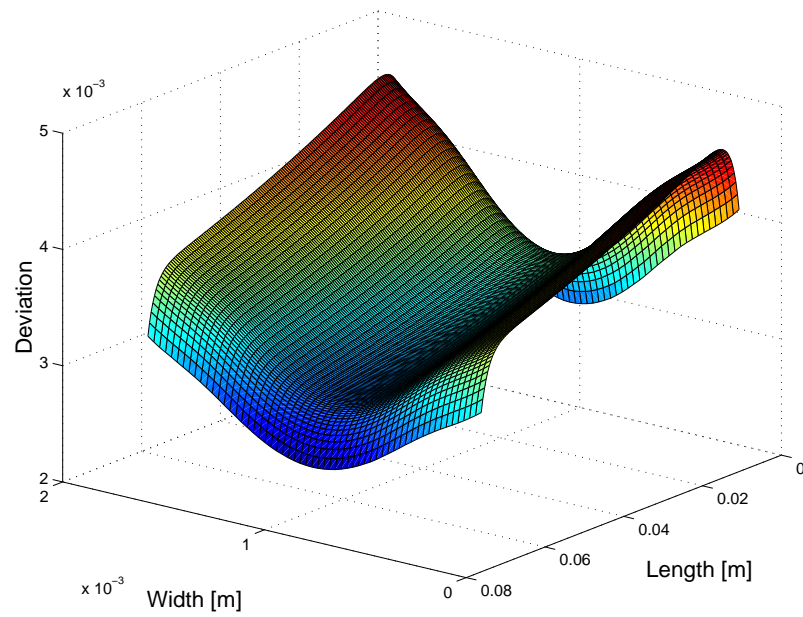


Figure 4.10: Relative difference in the local current density between the simulations using two different temperature boundaries (Reference constant temperature boundaries)

4.5 Current Density Distribution

It is difficult to properly visualise the processes taking place in the fuel cell. Thus the following plots have been made to illustrate the effects of concentration and activity on the current density distribution.

As seen in Figure 4.11 and 4.12, the current density distribution for the cathode side of the fuel cell (in this model the overpotential is assumed to be constant at the anode side) varies significantly with the load. For lower potentials (low loads) at the cathode the profiles of the activation overpotential and the local current density are fairly uniform. At higher loads the activation overpotential and the local current density varies much more over the catalyst layer. Both figures shows that the current density profile is more dependent on the activation overpotential than on the oxygen concentration.

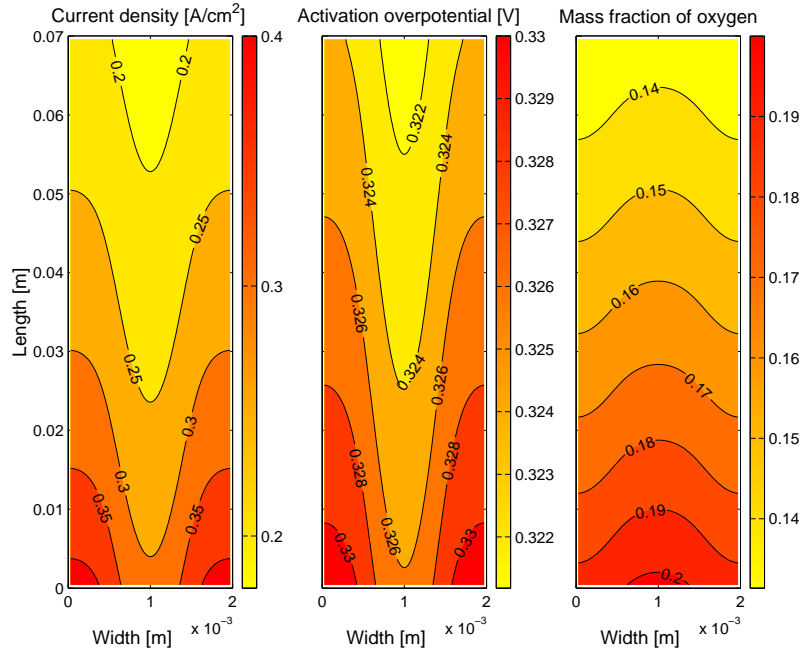


Figure 4.11: Profiles for current density, activation overpotential and oxygen mass fraction at the cathode catalyst layer at $V_{ref} = 15.444V$, $\beta = 0.5$

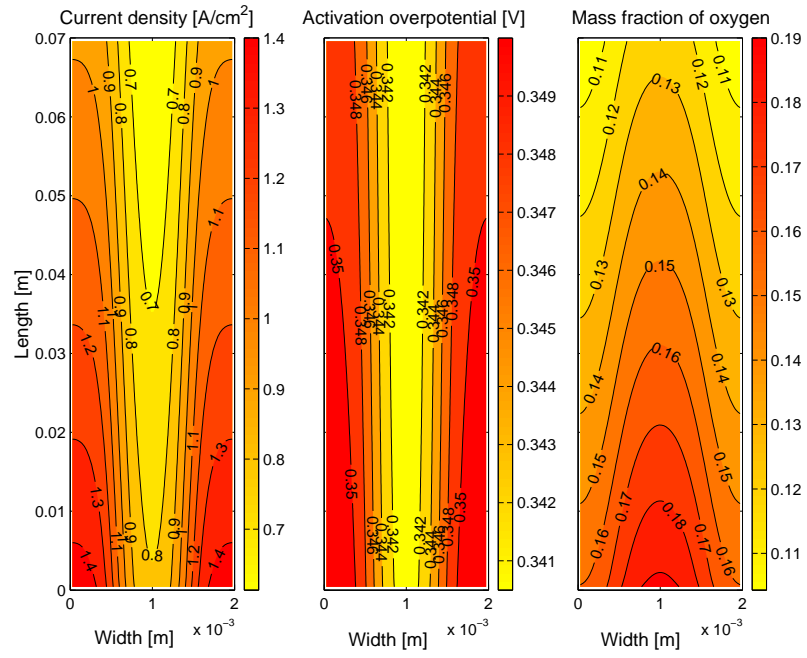


Figure 4.12: Profiles for current density, activation overpotential and oxygen mass fraction at the cathode catalyst layer at $V_{ref} = 15.405V$, $\beta = 0.5$

These results are radically different from the intuitively expected profile, where the current density should be highest in the centre of the channel where the concentration of reactants is highest. The predicted current density distribution is also fundamentally different from the current density distributions obtained with many of the previous 2D and 3D models [2][12][46], in which the surface overpotential is assumed constant and the local current density is directly related to the local reactant concentration. In these models, the highest current densities were found in the middle of the channel where the oxygen concentration is highest. However, Bang et al. recently published a three-dimensional model [44], with distributed activation potential and complete charge transport, which predicts similar results to this model. (C. Y. Wang et al. [47] have also recently published work that provides similar profiles).

The maximum current density occurs under the land area since the ohmic losses in the gas diffusion layer influence the activity at the catalyst more than the concentration losses. The electron path from the area of the catalyst layer which is under the flow channel is longer than the path from the area of the catalyst layer which is under the land areas (see Figure 2.1). If the conductivity is increased, the losses related to the transport of electrons from the area under the flow channel becomes smaller. Hence, the activation overpotential in this area increases and thus the local current density increases.

This can be illustrated by exploring the effect of increasing the electronic conductivity in the gas diffusion layer. A qualitative comparison between different electronic conductivities has been preformed. Since the fuel cells will operate at different loads (same cathode half cell potential) when the conductivity in the gas diffusion electrode is changed, relative current density profiles are examined. Figure 4.13(a), 4.13(b) and 4.13(c) shows how the relative current density profile changes when the resistance in the gas diffusion layer is reduced. The electronic conductivity is set to $100S/m$ [39],

825S/m [44] and 1500S/m respectively, all other parameters are unchanged.

When the electronic conductivity in the diffusion electrodes is increased (or the electrode thickness is reduced), the loss through the electrode is decreased. As the concentration losses becomes larger relative to the ohmic losses, the maximum current density moves toward the centre of the channel where the losses are smallest.

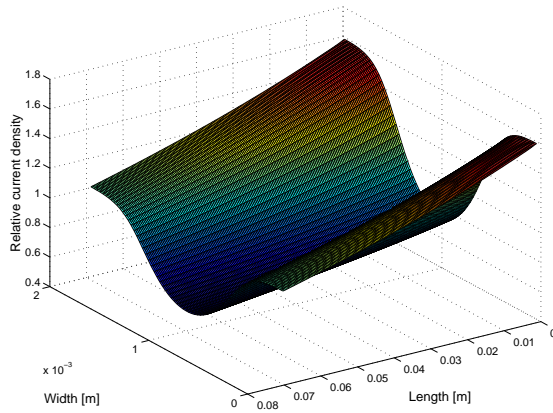
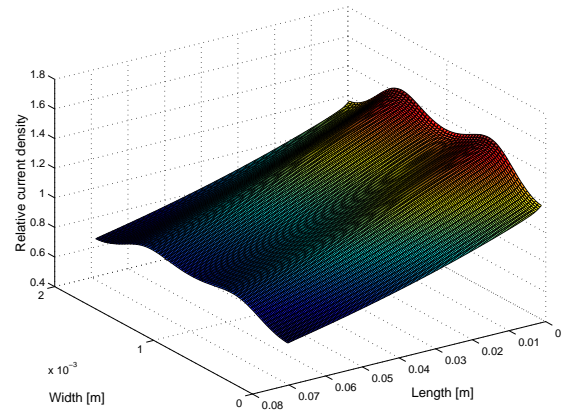
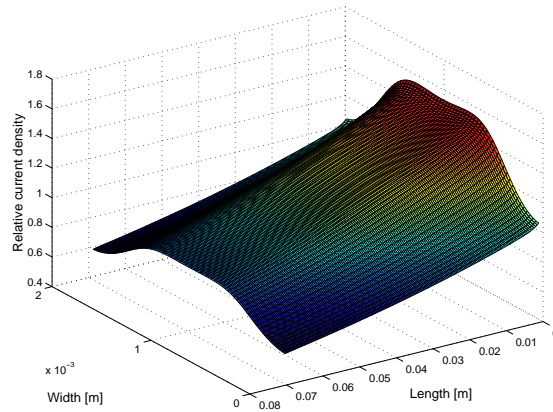
(a) Electric conductivity= $100S/m$ (b) Electric conductivity= $825S/m$ (c) Electric conductivity= $1500S/m$

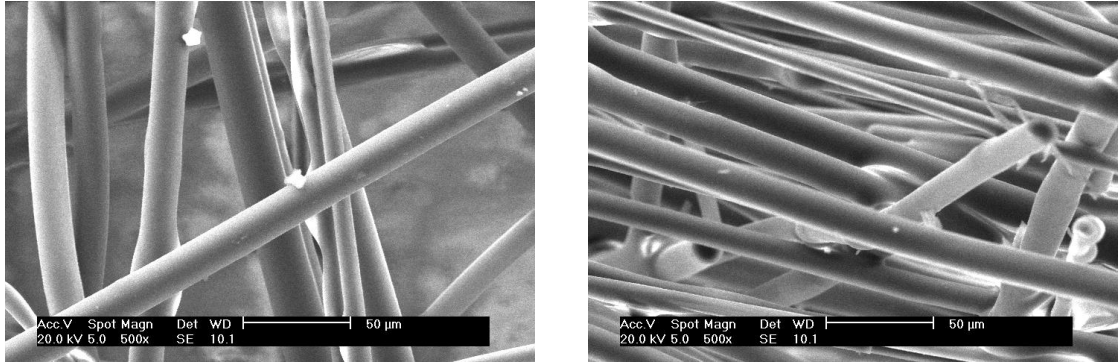
Figure 4.13: Plots of the relative current densities (i_{local}/i_{avg}) for different conductivities

4.5.1 Discussion

It has been shown that the variation of potential distribution in the fuel cell is determining for the current density distribution. In this model two-phase flow has not been considered. That might have a large impact on the actual current profiles. At higher current densities the water production increases, and liquid water might form in the gas diffusion layer. Liquid water pockets are more likely to form under the land area [48][46]. This will prevent the reactant gas to diffuse into the catalyst layer and thereby reduce the current density in this area. The reduction of reactants under the land area will lead to lower current densities in these areas, which is reverse of the trends given by this model. However, it should be noted that for simulations corresponding to intermediate current densities where flooding is not expected to play a significant role, the result is expected to be physical representative.

In this model the gas diffusion layer is assumed to be homogeneous and isotropic. In reality the carbon paper which is commonly used as the gas diffusion layer is not isotropic [20]. This can be illustrated by the pictures taken by Jim Irving at the Royal Military College of Canada, Dept. of Chemistry and Chemical Engineering, which is shown in Figure 4.14(a) and 4.14(b) [20]. Figure 4.14(a) is an image normal to a gas diffusion electrode, magnified 500 times. While Figure 4.14(b) shows the edge of the same gas diffusion electrode, also magnified 500 times. It can be seen that the fibres are much closer together in the plane of the gas diffusion electrode, than in the normal direction.

The permeability is more likely to be lower along the carbon paper than across it. This means that the species transport is lower in the tangential direction than perpendicular to the gas diffusion layer, due to lower flow. However, a more important effect of the non-isotropic gas diffusion layer is that the tortuosity factor will be different in the two directions. The tortuosity factor should be higher in the tangential



(a) In the direction normal to the plane

(b) In the direction of the plane

Figure 4.14: Magnified image of a gas diffusion electrode (Reproduced by premission from B. Peppley [20])

direction than perpendicular to the gas diffusion layer. This leads to a lower diffusion into the areas under the land areas. A more realistic modelling of the gas diffusion layer will therefore give lower concentration of reactant gas under the land area. Hence, lower local current densities in this area.

On the other hand, a case with serpentine flow channels could have a flow from one channel to the next through the gas diffusion layer [37]. This will increase the concentration of reactant gas under the land area and thereby increase the local current density in these areas. A higher current density under the land areas will again give a current density profile which is in accordance with the results given by this model.

An other important parameter which is not considered in this model, is that the conductivity of the membrane is dependent of the water content in the membrane. Intuitively, the water content should be lower under the flow channels than under the land areas, due to shorter transport path through the gas diffusion layer. This would probably lead to a lower local current density under the flow channel area, because

of a lower conductivity in a partly dehydrated membrane.

This short discussion show that the transport mechanisms taking place in the fuel cell are very complex, and highly dependent on each other. Further studies should be conducted to investigate the effect of two phase flow and non-isotropic diffusion layer. However, this model provides useful information on the trends in the fuel cell. It also shows that the current density profile, will look fundamentally different whether the variation in overpotential and ohmic loss in the electrodes are taken into account or not.

4.6 Losses

4.6.1 Ohmic losses in the electrodes

The potential field in the cathodic and the anodic gas diffusion electrode is shown in Figure 4.15 and 4.16 at an average current density of $0.989A/cm^2$. The profiles presented here is similar to the one obtained by Bang et al. [44].

It can be seen that the potential field lines are normal to the flow channel and the side walls, while there is a gradient into the land area where the electrons are transported into the bipolar plate. At the catalyst layer there is a gradient in both the x, y and z direction due to a nonuniform local current production. These profiles are in accordance with what was expected.

The effect of the ohmic loss in the gas diffusion electrode is discussed in section 4.5. In the same vein, Figure 4.15 shows that ohmic losses are larger in the area of the catalyst layer which is under the flow channel, due to longer transport path for the electrons.

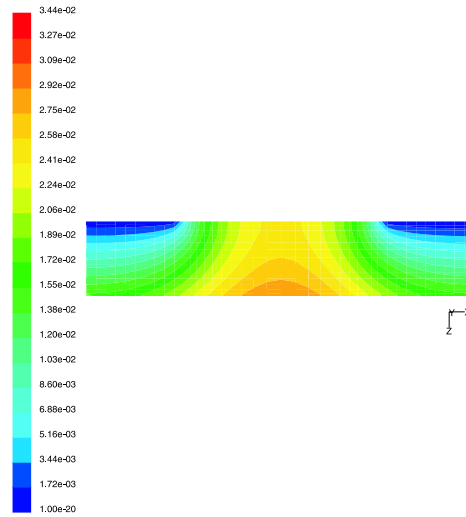


Figure 4.15: Potential profile through the cathodic diffusion electrode shown at a cross-section at the centre of the channel, $V_{ref} = 15.405V$, $\beta = 0.5$

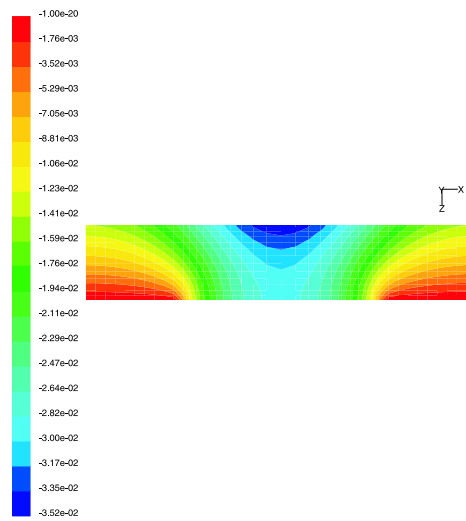


Figure 4.16: Potential profile through the anodic diffusion electrode shown at a cross-section at the centre of the channel, $V_{ref} = 15.405V$, $\beta = 0.5$

4.6.2 Ohmic losses in the membrane

The potential drop through the membrane at a cross-section in the centre of the channel, is presented in Figure 4.17 at an average current density of $0.989 A/cm^2$ and cathode half cell voltage of $15.405 V$. (The figure is scaled with a factor of 0.3 in the x-direction).

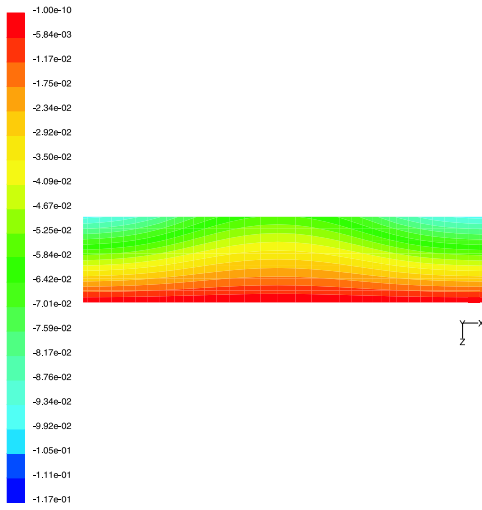


Figure 4.17: Potential profile through the membrane shown at a cross-section at the centre of the channel, $V_{ref} = 15.405 V$, $\beta = 0.5$

It can be seen that the potential at the anode side (bottom) is assumed to be uniform, and therefore used as a reference ($V_{mem} = 0 V$). The potential drop through the membrane corresponds to the local current production at the cathodic catalyst layer, where the local current density is highest under the land areas (see Figure 4.12).

4.6.3 Relative share of different losses

In this model it is possible to discern the relative share of the different overpotentials contributions. Figure 4.18 and 4.19 presents the relative share of activation overpotentials and the ohmic losses in the fuel cell, at a cathodic half cell potential of $15.444V$ and average current density of $0.269A/cm^2$ using different asymmetry parameters (diffusion losses are not considered in this figures).

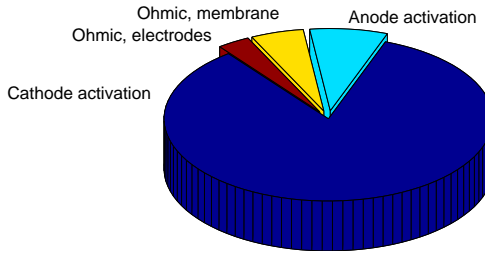


Figure 4.18: Share of overpotential contributions at $V_{ref} = 15.444V$, $\beta = 1.0$, $i_{avg} = 0.299A/cm^2$

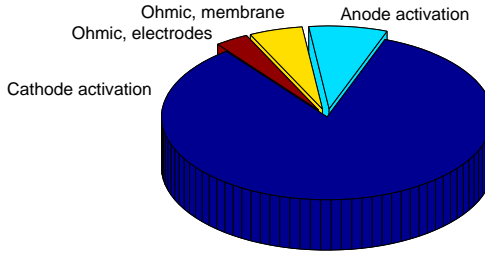


Figure 4.19: Share of overpotential contributions at $V_{ref} = 15.444V$, $\beta = 0.5$, $i_{avg} = 0.299A/cm^2$

Using an asymmetry parameter of $\beta = 1.0$; the cathodic activation overpotential is 0.8395% of the losses. With an asymmetry parameter of $\beta = 0.5$; the cathodic activation overpotential represents 0.8390% of the irreversibilities. At low current densities it can be seen that also average losses are very similar for the two different asymmetry parameters. However, the local losses will be different as illustrated in Figure 4.4.

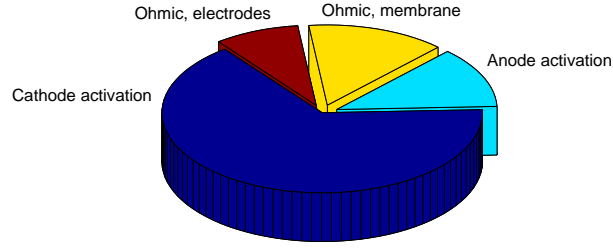


Figure 4.20: Share of overpotential contributions at $V_{ref} = 15.405V$, $\beta = 0.5$, $i_{avg} = 0.989A/cm^2$

Figure 4.20 shows the relative share of activation overpotentials and the ohmic losses in the fuel cell, at an average current density of $0.989A/cm^2$ and the asymmetry parameter equal to 0.5. It can be seen that the contribution of the ohmic losses are increasing as the average current densities are increased. The cathodic activation overpotential has decreased to 0.6520% of the relative share.

The magnitude of the various loss components is highly dependent of the parameters used in the model. A change in k_a , k_c , membrane conductivity or electronic conductivity in the gas diffusion electrode will alter the share/distribution among the different losses. However, the model gives an indication of the trends as the average current densities increases. The relative share of the overpotential contributions are in the same range, and the change in contribution at higher current densities are showing the same trends as the results obtained by Maggio et al. [49].

Chapter 5

Conclusions and Future Work

5.1 Conclusions

A three dimensional model of a Proton Exchange Membrane (PEM) Fuel Cell has been developed in the framework of a computational fluid dynamics (CFD) code. The model has been implemented, using the parallel processing architecture of the CFD code, to allow fast simulations even with large computational domains. The model accounts for the fluid transport inside the channels and the gas diffusion electrodes as well as heat transfer. The local current density is predicted in both the anodic and the cathodic catalyst layer, with a distributed overpotential at the cathode. Qualitative comparison has been made between results obtained with the model and experimental results. Good agreement was obtained when examining the polarisation curves. However, the results obtained using two different asymmetry parameters show that even though the model produces very similar polarisation curves, the current density distribution can be very different. This obviously shows, that a comparison between experimental and predicted polarisation curves is not sufficient to validate the model.

The predicted distribution of current densities shows profiles which are fundamentally different from the distribution obtained by many 2D and 3D models that do not take into account distributed overpotentials. The maximum current density occurs under the land area since the ohmic losses in the gas diffusion layer influence the activity at the catalyst greater than the concentration losses. The electron path from the area of the catalyst layer which is under the flow channel is longer than the path from the area of the catalyst layer which is under the land areas. If the conductivity is increased, the losses related to the transport of electrons from the area under the flow channel becomes smaller. Hence, the activation overpotential in this area increases and thus the local current density increases.

In this study it has been demonstrated that the current density profiles can be radically changed by changing for example the conductivity in the gas diffusion electrodes.

The grid study performed in this thesis shows that care should be taken when meshing a geometry. For a simple straight channel case with fully developed flows, the number of computational cells can be reduced without losing vital information. However, it is shown that the error is increasing down the channel, so a more complex geometry might need relatively much more computational cells. A grid study should be preformed in each case.

5.2 Future Work

The results obtained from the model presented in this thesis, demonstrates how modelling can provide insight and shed light on many of the transport processes taking place in a fuel cell. The development of physically representative models that allow reliable simulation of the processes under realistic conditions, is essential to the development of better fuel cells that have optimised performance and that can be manufactured using cheaper materials and techniques. However, the model presented in this thesis can by no means be considered complete.

In order to further improve the fuel cell model, there are several improvements and extensions that should be considered. Through out this thesis numerous issues have been pointed out. Some of the issues should be investigated further:

- The transport of protons through the catalyst layer at higher current densities should be included. At higher current densities the reaction zone tends to move in the catalyst layer, away from the membrane. This would lead to higher losses, due to lower conductivity of protons in the catalyst layer. By including this in the model, the predicted results at higher current densities will be more realistic.
- Include a better model for the membrane. Especially at higher current densities, the membrane can not be assumed to be fully humidified. A partly dehumidified membrane will have lower conductivity of protons, which will lead to higher and different distributed losses in the membrane, as well as different temperature distributions.
- Include a non-isotropic and non-homogeneous implementation of the gas diffusion electrodes. The gas diffusion electrodes are likely to have a much lower

permeability along the carbon paper than across it. The tortuosity factor will also vary with the direction. This will give a lower transport of reactants into the catalyst layer under the land area, which will interfere with the current density distribution.

- Including a two-phase model should be considered. At higher current densities liquid water is likely to form in the fuel cell, preventing the transport of reactants into the catalyst layer. This might also affect the current density distribution in the fuel cell.

References

- [1] A. Pollack. California upholds rules for pollutionless car by '03. *New York Times*, 9 September 2000.
- [2] T. Berning. *Three-Dimensional Computational Modelling of Transport Phenomena in PEM Fuel Cell*. PhD thesis, University of Victoria, 2002.
- [3] D. M. Bernardi and M. W. Verbrugge. Mathematical model of gas diffusion electrode bonded to a polymer electrolyte. *AIChE Journal*, 37(8):1151–1163, 1991.
- [4] D. M. Bernardi and M. W. Verbrugge. A mathematical model of the solid-polymer-electrolyte fuel cell. *J. Electrochem. Soc.*, 139(9):2477–2491, 1992.
- [5] A. Rowe and X. Li. Mathematical modeling of proton exchange membrane fuel cell. *Journal of Power Source*, 102:82–96, 200.
- [6] T. E. Springer, T. A. Zawodzinski, and S. Gottesfeld. Polymer electrolyte fuel cell model. *J. Electrochem. Soc.*, 138(8):2334–2342, 1991.
- [7] T. F. Fuller and J. Newman. Water and thermal management in solid-polymer-electrolyte fuel cells. *J. Electrochem. Soc.*, 140(5):1218–1225, 1993.
- [8] T. V. Nguyen and R. E. White. A water and heat management model for proton-exchange-membrane fuel cells. *J. Electrochem. Soc.*, 140(8):2178–2186, 1993.

- [9] J. S. Yi and T. V. Nguyen. An along-the-channel model for proton exchange membrane fuel cells. *J. Electrochem. Soc.*, 145(4):1149–1159, 1998.
- [10] V. Gurau, H. Liu, and S. Kakaç. Two-dimensional model for proton exchange membrane fuel cells. *AIChE Journal*, 44(11):2410–2422, 1998.
- [11] S. Dutta, S. Shimpalee, and J. W. Van Zee. Three-dimensional numerical simulation of straight channel PEM fuel cells. *Journal of Applied Electrochemistry*, 30:135–146, 2000.
- [12] T. Berning, D. M. Lu, and N. Djilali. Three-dimensional computational analysis of transport phenomena in a PEM fuel cell. *Journal of Power Sources*, 106:284–294, 2002.
- [13] É. Turgeon, D. Pelletier, and J. Borggaard. Sensitivity and uncertainty analysis for variable flows. In *39th AIAA Aerospace Sciences Meeting and Exhibit*, Reno, NV, 2001. AIAA. AIAA 2001-0139.
- [14] J. Borggaard, J. F. Héту, and D. Pelletier. Sensitivity and uncertainty analysis for conjugate phase-change problems. In R. M. Barron, editor, *The 10th Annual Conference of the CFD Society of Canada, Proceedings*, pages 66–71, Windsor, Ontario, 2002.
- [15] J. Larminie and A. Dicks. *Fuel Cell Systems Explained*. John Wiley and Sons, Ltd, 2000.
- [16] B. R. Sivertsen. Background for modelling of a proton exchange membrane fuel cell. Project conducted at University of Victoria, Institute for Integrated Energy Systems, in partial fulfilment of the requirements for the degree in Master of Science, 2002.

- [17] Z. H. Wang, C. Y. Wang, and K. S. Chen. Two-phase flow and transport in the air cathode of proton exchange membrane fuel cells. *Journal of Power Sources*, 94:40–50, 2000.
- [18] A. F. Mills. *Heat Transfer*. Prentice Hall, second edition, 1999.
- [19] Fluent Incorporated. *Fluent 6.0 and 6.1 User's Guide*, 2001.
- [20] J. G. Pharoah. Queen's university. personal communication, 2003.
- [21] Y. A. Çengel and M. A. Boles. *Thermodynamics: An Engineering Approach*. McGraw-Hill, second edition, 1994.
- [22] L. Wang, A. Husar, T. Zhou, and H. Liu. A parameteric study of PEM fuel cell performances. *International Journal of Hydrogen Energy*, 2003. Article in Press.
- [23] M. J. Lampinen and M. Fomino. Analysis of free energy and entropy changes for half-cell reactions. *J. Electrochem. Soc.*, 140(12):3537–3546, 1993.
- [24] H. K. Versteeg and W. Malalaeskera. *An introduction to computational fluid dynamics The finite volume method*. Prentice Hall, 1995.
- [25] F. M. White. *Fluid Mechanics*. WCB/McGraw-Hill, fourth edition, 1999.
- [26] E. L. Cussler. *Diffusion Mass Transfer in Fluid Systems*. Cambridge University Press, second edition, 1997.
- [27] R. Taylor and R. Krishna. *Multicomponent Mass Transfer*. John Wiley and Sons, 1993.
- [28] W. Kast and C.-R. Hohenthanner. Mass transfer within the gas-phase of porous media. *International Journal of Heat and Mass Transfer*, 43:807–823, 2000.

- [29] C. H. Hamann, A. Hamnett, and W. Vielstich. *Electrochemistry*. Wiley-VCH, 1998.
- [30] R. C. Weast, editor. *CRC Handbook of Chemistry and Physics*. CRC Press, Inc., 70th edition, 1989.
- [31] M. J. Lampinen and M. Fomino. Analysis of different energy scales in chemical thermodynamics and estimation of free energy and enthalpy changes for half cell reactions. *Acta polytechnica Scandinavica*, 1993. Chemical Technology and Metallurgy Series No.213, Helsinki 1993.
- [32] Y. Sone, P. Ekdunge, and D. Simonsson. Proton conductivity of Nafion 117 as measured by a four-electrode AC impedance methode. *J. Electrochem. Soc.*, 143(4):1254–1259, 1996.
- [33] G. J. M. Janssen. A phenomenological model of water transpot in a proton exchange membrane fuel cell. *Journal of The Electrochemical Society*, 148(12):A1313–A1323, 2001.
- [34] F. M. White. *Viscous Fluid Flow*. McGraw-Hill Series in Mechanical Engineering. McGraw-Hill, Inc., second edition, 1991.
- [35] S. Kakaç, R. K. Shah, and W. Aung, editors. *Handbook of Single-Phase Convective Heat Transfer*. John Wiley and Sons, Inc., 1987.
- [36] M. J. Moran and H. N. Shapiro. *Fundamentals of Engineering Thermodynamics*. John Wiley and Sons, 1996.
- [37] S. Dutta, S. Shimpalee, and J. W. Van Zee. Numerical prediction of mass-exchange between cathode and anode channels in a PEM fuel cell. *International Journal Heat and Mass Transfer*, 44:2029–2042, 2001.

- [38] S. Shimpalee and S. Dutta. Numerical prediction of temperature distribution in PEM fuel cells. *Numerical Heat Transfer*, 38:111–128, 2000. Part A.
- [39] A. Fischer, J. Jindra, and H. Wendt. Porosity and catalyst utilization of thin layer cathodes in air operated PEM-fuel cells. *Journal of Applied Electrochemistry*, 28:277–282, 1998.
- [40] N. Djilali and D. Lu. Influence of heat on gas and water transport in fuel cells. *International Journal of Thermal Sciences*, 41:29–40, 2002.
- [41] A. J. Bard and L. R. Faulkner. *Electrochemical Methods, Fundamentals and Applications*. John Wiley and Sons, second edition, 2001.
- [42] E. Middelmann, W. Kout, and B. Vogelaar. Bipolar plates for PEM fuel cells. *Journal of Power Sources*, 2003. Article in Press.
- [43] T. Berning and N. Djilali. A three-dimensional, multi-phase, multicomponent model of the cathode and anode of a PEM fuel cell. *J. Electrochem. Soc.*, 2003. Article in Press.
- [44] M. Bang, S. Yde-Andersen, T. J. Condra, N. Djilali, and E. Skou. Modelling of potential fields and electrochemical reactions in PEM fuel cells. In *Proceedings of Hydrogen and Fuel Cells, Conference and Trade Show*, Vancouver, Canada, June 2003. In Press.
- [45] L. You and H. Liu. A two-phase flow and transport model for the cathode of PEM fuel cells. *International Journal of Heat and Mass Transfer*, 45:2277–2287, 2002.
- [46] M. J. Kermani, J. M. Stockie, and A. G. Gerber. Condensation in the cathode of a PEM fuel cell. In *Proceedings of the 11th Annual Conference of the CFD Society of Canada*, volume 1, pages 292–299, Vancouver, Canada, May 2003.

- [47] C. Y. Wang. Transport issues in polymer electrolyte fuel cell. In *Purdue Heat Transfer Celebration*, 2003.
- [48] D. Natarajan and T. V. Nguyen. Three-dimensional effects of liquid water flooding in the cathode of a PEM fuel cell. *Journal of Power Sources*, 115:66–80, 2002.
- [49] G. Maggio, V. Recupero, and L. Pino. Modeling polymer electrolyte fuel cells: an innovative approach. *Journal of Power Sources*, 101:275–286, 2001.
- [50] S. Trasatti. The "absolute" electrode potential-the end of the story. *Electrochimica Acta*, 35(1):269–271, 1990.

Appendix A

Half-cell Voltage

The electrical work associated with the electrochemical half-cell reaction is [23]:

$$L_{el} = zFE \quad (\text{A.1})$$

in which z can be understood as the number of electrons taking part in the half-cell reaction. If the positive charge of the electrode is increased, then z is defined to be positive and consequently if the charge of the electrode is decreased z is defined to be negative. F is the Faraday's constant and E is the cell voltage.

According to the first law of thermodynamics, the energy balance for half-cell reaction might be written as [23]:

$$Q_{in} = \Delta H - L_{el} \quad (\text{A.2})$$

where

$$\Delta H = \Delta U + p\Delta V \quad (\text{A.3})$$

in which Q_{in} is the absorbed heat from the surroundings, ΔH is the entropy change

in the system, ΔU is the change in internal energy and $p\Delta V$ is the expansion work. From the second law of thermodynamics [36]:

$$T\Delta S \geq Q_{in} \quad (\text{A.4})$$

where T is the temperature, and ΔS is the entropy change. If equation (A.4) and (A.3) are inserted into equation (A.2), the following equation can be obtained:

$$L_{el} \leq \Delta G \quad (\text{A.5})$$

where ΔG is the pure chemical free energy, not including the electrostatic energy [23]. The total free energy for the reaction can be expressed as [23]:

$$\Delta G_{tot} \equiv \Delta G + L_{el} \leq 0 \quad (\text{A.6})$$

For a reversible process the equal sign is valid in equation (A.4). Hence, the equal sign is also valid in equation (A.5) and (A.6).

The half-cell voltage is a function of the pure chemical free energy, which is given by [23][31]:

$$\Delta G = \sum_{i \in R} v_i \mu_i - z\mu[e^-(M)] \quad (\text{A.7})$$

where v_i are stoichiometric coefficients, μ is the chemical potential and $\mu[e^-(M)]$ is the chemical potential of the electrons, $\mu^\circ[e^-(M)]$ is dependent of the catalyst material M , species $i \in R$ does not include electrons, and the other electrochemical standard potential can be found tabulated. In electrochemistry the zero points at standard state are defined as [23][31]:

$$\mu^\circ[H_2(g)] \equiv 0 \quad (\text{A.8})$$

$$\mu^\circ[H^+(aq)] \equiv 0 \quad (\text{A.9})$$

From these relations, the Gibb's free energy for platinum electrodes can be found and the half-cell potential computed.

For a multicomponent system the chemical potential is [36]:

$$\mu_i = \bar{g}^\circ + RT \ln a_i \quad (\text{A.10})$$

where R is the general gas constant and a_i is the activity of component i .

For ideal gases it can be shown that the activity, a_i , can be written as [15]:

$$a_i = \frac{p_i}{p^\circ} \quad (\text{A.11})$$

in which p_i is the partial pressure of the gas and p° is the standard pressure, 0.1MPa.

The activity of water vapour, is given as [15]:

$$a_i = \frac{p_i}{p_{w,sat}} \quad (\text{A.12})$$

in which $p_{w,sat}$ is the vapour pressure of steam at a given temperature.

The activity for dissolved ions can be expressed by the molality, m (mol/kg), which is a measure of the concentration [29]:

$$a_i = \gamma_i \frac{m_i}{m^\circ} \quad (\text{A.13})$$

where γ_i is the activity coefficient and represents the deviation from ideality. At infinite dilution, where there are no inter-ionic interactions, $\gamma_i = 1$. m° is the standard concentration and is taken to be 1 mol/kg [29].

It is assumed that the electrons are in their standard state and hence the activity

is equal to 1.

For a system containing four active components, A, B, C and D, the reaction can be written as:



where the ν 's are stoichiometric coefficients.

The molar free energy, ΔG , of the reaction is given by [29]:

$$\Delta G = \sum_i \nu_i \mu_i \quad (\text{A.15})$$

The stoichiometric numbers, ν_i , of the reactants are assigned negative values and the products are assigned positive values. At equilibrium, the free energy must be zero. Otherwise it will be possible to lower the free energy of the mixture by letting the reaction proceed in one of the directions towards equilibrium [29].

For a system in equilibrium, $dG|_{T,p} = 0$, the equation of equilibrium for reaction (A.14), can be written as [36]:

$$\nu_A \mu_A + \nu_B \mu_B = \nu_C \mu_C + \nu_D \mu_D \quad (\text{A.16})$$

When employing equation (A.10) into equation (A.16) and rearranging the terms the result can be written as [36]:

$$\Delta G^\circ = -RT \ln \left(\frac{a_C^{\nu_C} a_D^{\nu_D}}{a_A^{\nu_A} a_B^{\nu_B}} \right) = -RT \ln K \quad (\text{A.17})$$

where K is defined as the equilibrium constant.

For a system that is not in equilibrium, it can similarly be shown, by inserting

equation (A.10) in equation (A.15), that the Gibb's function per mole is [15]:

$$\Delta\bar{g} = \Delta\bar{g}^\circ + RT \ln \left(\frac{a_C^{\nu_C} a_D^{\nu_D}}{a_A^{\nu_A} a_B^{\nu_B}} \right) \quad (\text{A.18})$$

This makes it possible to calculate the Gibb's free energy change at different temperatures, pressures and compositions of reactants and products.

As shown above, for an ideal system the Gibb's free energy change equals the electrical work done, which is equal to the charge times the voltage. This can be expressed generally as [15]:

$$\Delta\bar{g} = -nFE \quad (\text{A.19})$$

where n is the number of electrons, F is Faraday's constant and E is the cell voltage. Inserting this into equation (A.18) gives what usually is referred to as the Nernst equation [15]:

$$E_r = E^\circ - \frac{RT}{nF} \ln \left(\frac{a_C^{\nu_C} a_D^{\nu_D}}{a_A^{\nu_A} a_B^{\nu_B}} \right) \quad (\text{A.20})$$

where E_r is the reversible cell voltage and E° is the open circuit voltage at standard pressure.

For a platinum catalyst in standard state it can be shown that the $\mu^\circ[e^-(Pt)] = 1414.98 kJ/mol$ [23]. For the anode in a PEM fuel cell (see reaction 1.1) at standard states, it can be calculated that $\Delta G_a = 2829.0 kJ/mol$ which gives a cell potential $E_a = 14.66V$. For the cathode in a PEM fuel cell (see reaction 1.2), also at standard states, $\Delta G_c = 3066.15 kJ/mol$ and $E_c = 15.88V$ [23]. For an entire cell reaction the Gibb's free energy can be calculated as:

$$\Delta G_{tot} = \Delta G_a - \Delta G_c \quad (\text{A.21})$$

and the fuel cell potential can be derived from the relation [29] [50]:

$$\Delta E = E_c - E_a \quad (\text{A.22})$$

This gives for the whole cell $\Delta G_{tot} = -237.15 kJ/mol$ and $E = 1.229$. If Gibb's free energy is calculated for the total reaction, in the fuel cell, using standard values $\Delta G = -237.19 kJ/mol$ [23] and $E = 1.229V$ calculated from standard potentials [29]. This shows that the method described by Lampinen et al. [23] can be used to calculate the electrode potentials and half-cell free energy.

Appendix B

Heat and Entropy for Half-cell Reactions

The majority of this appendix is taken from the project conducted fall 2002 [16].

The heat in a fuel cell is generated due to changes of enthalpy and irreversibilities related to charge transfer. In order to calculate the heat generation in each electrode reaction, both charged and non-charged species need to be considered.

From the first law of thermodynamics, the energy balance for a half-cell can be written as [23]:

$$\dot{q} = r\Delta H + P_{el} \quad (\text{B.1})$$

where \dot{q} is the heat absorbed, r is the reaction rate of the half cell reaction, ΔH is the half cell reaction enthalpy and P_{el} is the electrical power. The reaction rate can be expressed as a function of the current density [23]:

$$r = \frac{i}{nF} \quad (\text{B.2})$$

in which i is the current density, n is the number of electrons transferred, F is Faraday's constant.

The electrical power generation associated with the electrochemical half-cell reaction is:

$$P_{el}'' = V \cdot i = \frac{-\Delta G}{nF} i \quad (\text{B.3})$$

where ΔG is the change in Gibbs free energy.

For a real irreversible process this gives [23]:

$$\dot{q} = |i/nF|(\Delta H + (-\Delta G)) - |i||\eta| = |i/nF|(T\Delta S) - |i||\eta| \quad (\text{B.4})$$

in which the last term represents the irreversibilities associated with the electrochemical reaction and the electron transport. η is the voltage drop (overpotential) due to ohmic losses and reaction resistance and ΔS is the entropy change for the half cell reaction. Lampinen and Fomino [23][31] present a method of how to calculate the half-cell entropy change.

Lampinen et al. introduce a semi-absolute entropy, f , for charged species, with a defined arbitrary zero point

$$f^\circ[H^+(aq)] \equiv 0 \quad (\text{B.5})$$

This is different from the regularly used absolute entropy, s , where the entropy is zero for any pure element at the temperature of absolute zero. It should be emphasised that

$$f^\circ[H^+(aq)] \neq s^\circ[H^+(aq)]$$

The absolute entropy of specie i at pressure p and temperature T can be calculated from [23]:

$$s_i(T, p) = s_i^\circ + \int_{T_0}^T \frac{c_{pi}}{T} dT + \int_{p_0}^p \left[\frac{\delta v_i}{\delta T} \right] dp \quad (\text{B.6})$$

and the corresponding semi-absolute entropy:

$$f_i(T, p) = f_i^\circ + \int_{T_0}^T \frac{c_{pi}}{T} dT + \int_{p_0}^p \left[\frac{\delta v_i}{\delta T} \right] dp \quad (\text{B.7})$$

The following thermodynamic relations are valid:

$$\frac{\partial f_i}{\partial T} = \frac{\partial s_i}{\partial T} = \frac{c_{pi}}{T} \quad (\text{B.8})$$

$$\frac{\partial f_i}{\partial p} = \frac{\partial s_i}{\partial p} = \frac{-\partial v_i}{\partial T} \quad (\text{B.9})$$

If specific heat is taken as constant, the two equations (B.6) and (B.7) can be expressed in the form [36]:

$$s_i(T, p) = s_i^\circ + c_{pi} \ln \frac{T}{T^\circ} - R \ln \frac{p}{p^\circ} \quad (\text{B.10})$$

For an ideal gas with the partial pressure, $p_i = x_i p$, the entropy of component i , at temperature T and reference pressure p_{ref} , takes the form [36]:

$$s_i(T, p_i) = s_i^\circ(T) - R \ln \frac{x_i p}{p^\circ} \quad (\text{B.11})$$

It can be shown that the total entropy of the system can be expressed as [23]:

$$S = \sum_{i=1}^k n_i s_i + \sum_{i=k+1}^m n_i f_i \quad (\text{B.12})$$

and that this equation is consistent with the equation for the systems entropy given by Moran et al. [36]:

$$\mathbf{S} = \sum_{i=1}^j n_i s_i \quad (\text{B.13})$$

For the anode reaction in a fuel cell the enthalpy of the electron at the platinum

catalyst can then be found as [23][31]:

$$f^\circ[e^-(Pt)] = 1/2s^\circ[H_2(g)] - f^\circ[H^+(aq)] \quad (\text{B.14})$$

If combined with equation (B.5), equation (B.14) becomes

$$f^\circ[e^-(Pt)] = 1/2s^\circ[H_2(g)] \quad (\text{B.15})$$

Lampinen and Fomino show that the value of the entropy for the electron at the platinum catalyst at the standard reference state is [23][36]:

$$f^\circ[e^-(Pt)] = 65.29J/molK$$

For the anodic reaction in a PEM fuel cell, at $T = 298.15K$: $\Delta G = 2829kJ/mol$, $\Delta S = 0.104J/molK$, $n = 2$ [23]. Assuming $i = 800A/m^2$ and $\eta = 0.20V$, the value of the heat source is obtained from equation (B.4):

$$\dot{q} = \frac{800A/m^2}{2 \cdot 96485C} \cdot (298.15K \cdot 0.104J/mol) - 800A/m^2 \cdot 0.20V = -159.87W/m^2$$

For some operation conditions this value might become positive and the anode acts as a heat sink.

For the cathodic reaction in a PEM fuel cell at $T = 298.15K$: $\Delta G = 6132.3kJ/mol$, $\Delta S = -326.36J/molK$, $n = 4$ [23]. Assuming $i = 800A/m^2$ and $\eta = 0.35V$, the value of the heat source is obtained from equation (B.4):

$$\dot{q} = -481.70W/m^2$$

The overall heat generation in the cell is the sum of the contribution from the two

half-cells and equals $-641.57W/m^2$.

The heat generation of the total cell can also be calculated directly, using the standard values for the total reaction: $\Delta G_{tot} = -237.19kJ/mol$, $\Delta S_{tot} = -162.8J/molK$ at $T = 298.15K$ and with $n = 2$ [23]. Using the same assumptions as above $i = 800A/m^2$ and $\eta_{tot} = 0.20V + 0.35V = 0.55V$:

$$\dot{q} = 640.48W/m^2$$

The result should be the same as the sum of the contributions from the two half-cells, but rounding errors leads to a small deviation.

Appendix C

Fluid Properties

Material	Specific heat [$J/kg \cdot K$]	Thermal conductivity [$W/m \cdot K$]	Viscosity [$kg/m \cdot s$]
Hydrogen	14590.0	0.21250	$9.865 \cdot 10^{-6}$
Oxygen	932.5	0.03110	$2.300 \cdot 10^{-5}$
Nitrogen	1045	0.02965	$1.960 \cdot 10^{-5}$
Water vapour	2014	0.02610	$1.340 \cdot 10^{-5}$

Table C.1: Fluid properties used in this model [18], $T = 353.15K$